SAND79-7097
Unlimited Release
UC-94b

Research and Development for Inertial Energy Storage Based on a Flexible Flywheel

Dr. John M. Vance

Issued by Sandia Laboratories, operated for the United States Department of Energy by Sandia Corporation.

RESEARCH AND DEVELOPMENT FOR
INERTIAL ENERGY STORAGE BASED
ON A FLEXIBLE FLYWHEEL

FINAL REPORT

Prepared by

Dr. John M. Vance
Department of Mechanical Engineering
Texas A&M University
College Station, Texas   77843

ABSTRACT

A design concept for a non-rigid energy-storage flywheel suitable for home or farm use has been investigated at Texas A&M University under a Sandia Laboratories' contract. The distinguishing feature of this "flexible flywheel" is its construction from high strength fibers (such as synthetic rope) with no bonding agent. The work done to date indicates that the flexible flywheel is self-balancing, safe, has a high energy-density capability (60 Wh/lb), and should be simple and economical to manufacture. The major thrust of the contract work has been to find a solution to the subsynchronous whirling instability, a problem common to all high speed flywheels, which is especially severe in the flexible flywheel due to the high supercritical speed ratio and the large amount of internal friction. A unique gimbal support system has been designed and analyzed and tested on this contract which stabilizes the flywheel without the need for a squeeze film damper. The conceptual design was developed for a flexible flywheel energy storage system suitable for interfacing with a small-scale solar energy source. Cost estimates were prepared for the system in the 10 KWh and 50 KWh sizes.

1-2
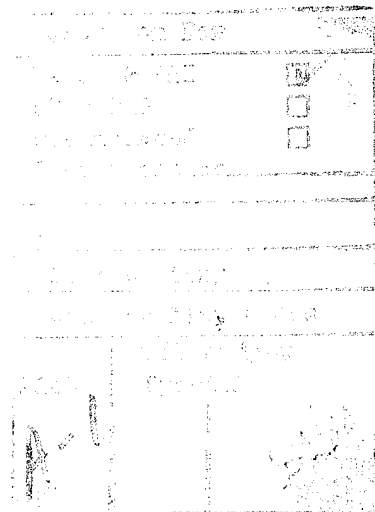
Acknowledgments

The Principal Investigator wishes to acknowledge the major contributions to this work by the following people:

Dr. Richard T. Schneider invented the flexible flywheel, did much of the setup and construction work for the vacuum chamber, and guided the economic analysis.

Mr. Brian Murphy developed the computer stability analysis, directed the research during a six week absence by the Principal Investigator, measured the torque capability of the support ropes, and correlated experimental results from the small model with computer predicted results.

Mr. Wallace Ables performed many of the experimental measurements and constructed most of the experimental apparatus.

Mr. B. Dudley Carter made the study of costs and economic factors for a flexible flywheel storage system.

A number of other people, too numerous to mention, also made valuable contributions. Their help is gratefully appreciated.

TABLE OF CONTENTS

LIST OF TABLES

5

LIST OF FIGURES

INTRODUCTION

In 1975, Dr. R. T. Schneider at the University of Florida conceived the idea of a flexible flywheel made of rope for energy storage. The idea was to develop an economical, safe, self-balancing energy storage device to make solar or wind-generated electricity practical for home or farm use.

Beginning in 1976, a flywheel test facility was constructed and the first rope flywheels were spun up. It soon became evident that one of the advantages of the flexible flywheel, its self-balancing feature, had been bought at the price of a subsynchronous whirling instability caused by internal friction. This poses a problem because the whirl critical speed is well below the operating speed range for the flywheel. The early test work on the flexible flywheel was carried out in the Nuclear Engineering Department at the University of Florida by Dr. Schneider and several other nuclear engineering students who had little or no experience or training in the field of rotor dynamics. In fact, it was not realized at first that the whirling was not synchronous and therefore not affected by rotor unbalance. One of the early unsuccessful efforts to control the whirling was by increasing the support rope constraints, an approach which rotor dynamics theory shows will actually aggravate the problem.

Since the major technical problem of the flexible flywheel was found to be one of rotor dynamics, the author of this report (who is active in this field) joined work on the project while in the Department of Mechanical Engineering at the University of Florida. The project was subsequently moved to Texas A&M University in 1978 when the author moved there, and all experiments and analyses described in this report were performed there.

SUMMARY

The flexible flywheel concept originated by Dr. R. T. Schneider at the University of Florida has been investigated experimentally and analytically at Texas A&M University. The flexible flywheel is constructed from synthetic rope with no bonding agent, and is flexibly supported (no hub) to induce self-balancing characteristics.

Three experimental flywheels were built and tested: a 10-1/2" diameter Nylon flywheel weighing 2.7 lb., a 22-1/2" diameter Dacron wheel weighing 19 lb., and a 30" diameter Nylon wheel weighing 88 lb. All three wheels were suspended by various support rope (and/or wire cable) configurations from a gimballed motor/generator support system designed to suppress subsynchronous whirl. In all cases the motor/generator was operated in the motor mode only.

The experiments demonstrated that the gimballed motor/generator support system has a strong stabilizing influence on flexible flywheel dynamics. Without the gimbals, all of the wheels always begin unstable whirling immediately above the first critical speed (typically about 50-100 rpm). In addition, it was found that whirl stability is sensitive to the support rope configuration. The most stable configuration was found to be twisted ("maypole") support ropes, approximating a synthetic quill shaft.

The most impressive feature of the flexible flywheel demonstrated by the experiments was self-balancing, a result of the flexible supports. None of the flywheels had to be balanced, and no noticeable synchronous vibration was ever transmitted to the structure.

Maximum speeds achieved with the three wheels were 2600 rpm (10-1/2" wheel), 2000 rpm (22-1/2" wheel) and 1500 rpm (30" wheel). With the twisted support ropes, these speed limits were imposed by electrical power supply limitations in overcoming air drag. With the untwisted ropes, speeds were

11

limited by the subsynchronous whirl instability threshold.

A computerized stability analysis was also developed to guide the design, improve understanding of the destabilizing mechanism, and ultimately to optimize the design parameters for dynamic stability. All of the predicted critical speeds and mode shapes agreed closely with experimental measurements, and the thresholds of stability could be accurately simulated by adjusting the (unknown) values of internal hysteresis in the mathematical model. One result of the analysis is a theory to rationally explain why the maypole configuration is stable and the untwisted support rope configuration is not.

In order to answer questions about the torque capacity of the twisted maypole support rope, measurements of the actual air drag torque on the 22 1/2" flywheel were made at various speeds which showed a power capability to generate more than 1.3 KW at 6,000 rpm, and more than 2.2 KW at 10,000 rpm. On several occasions during the experiments, the electrical current demand due to air drag caused circuit breakers to trip in the power supply, thus subjecting the flywheel to a severe transient decelerating torque. It was found that the flywheel could handle these transients with no unfavorable effects.

The production cost for a conceptual 50 KWh residential flexible flywheel energy storage system is estimated to be $24,160 ($483/KWh). Based on that cost estimate and using a life cycle cost methodology developed for solar energy systems, the residential present value cost ($1979) for this 50 KWh system would be $36,437.

Probably the most important conclusions to be drawn from this research are:

12

(1) Subsynchronous whirl instability at supercritical speeds due to internal friction is strongly suppressed by a gimballed motor/generator support system. (This finding is applicable to more conventional flywheels, as well as to the flexible flywheel.)

(2) A flexible flywheel made from synthetic rope or fiber with no bonding agent is easy to construct and can be made self-balancing by a properly designed support system.

(3) The flexible flywheel system offers a relatively inexpensive and efficient tool for investigating flywheel rotor dynamics in general, since:

    (a) failures are not catastrophic,

    (b) critical speeds are so low that whirl modes can be visually observed, and

    (c) support rope configurations can be varied to approximate the shaft constraints of conventional flywheels.

(4) The simplicity of the flexible flywheel construction promotes economical production using conventional manufacturing processes and equipment.

CONFIGURATION AND ADVANTAGES OF THE FLEXIBLE FLYWHEEL

Figure 1 shows a photograph of an early experimental flexible flywheel. Notice that the support ropes carry only the weight of the flywheel and that there is no rigid hub or spoke array as in a conventional solid or composite flywheel.

The radial ropes constraining the flywheel to the lower circular flange were intended to control whirling, an approach which was subsequently found to aggravate the problem. In the present design, radial stiffness of the rotor is provided by gravity only, as in a pendulum.

The flywheel is a simple hoop, constructed by coiling ropes or fibers in a circle of the desired radius until the design mass is achieved. At speed, centrifugal force maintains the circular configuration. For the sake of shape integrity when not spinning, one layer of rope is wound around the cross section of the hoop. (Early models were of macrame construction, but this was found to sacrifice strength with no apparent advantage.) The loose ends of the coiled hoop are joined by tying or splicing.

From the standpoint of energy density, this fiber/hoop configuration is the optimum attainable. It is obviously cheap to manufacture, and newly developed high strength fibers will be easy to incorporate into the design without the need to develop new bonding techniques.

The question of torque capacity and acceleration has been investigated for the support rope configuration shown in Figure 2 and appears not to be a problem. The most stable configuration (from the standpoint of whirling) occurs when the support ropes are twisted around each other. The torque capacity of this configuration has also been investigated and is ample for the high design speeds achievable with synthetic fibers.

15
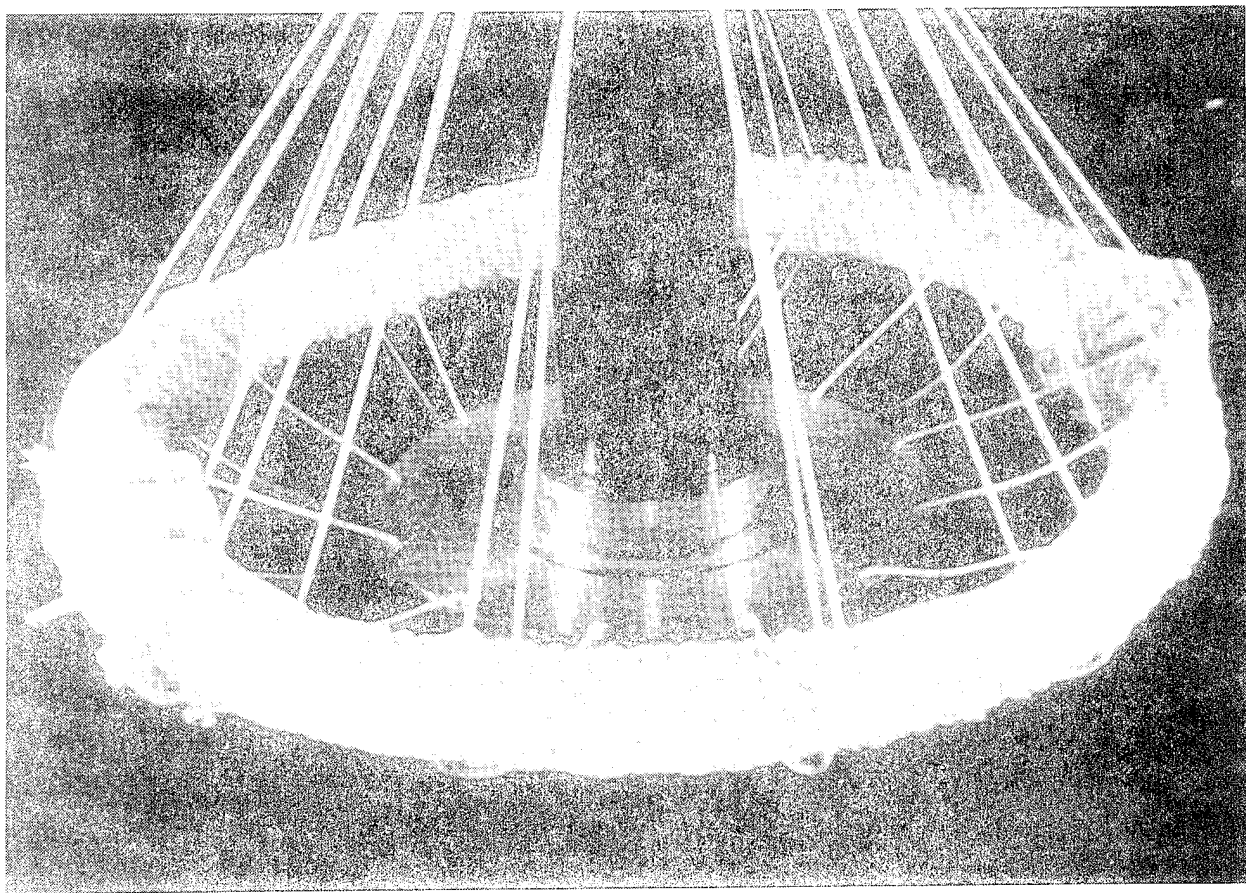
Fig. 1. Early Flexible Flywheel with Lower Radial-Constraint Ropes
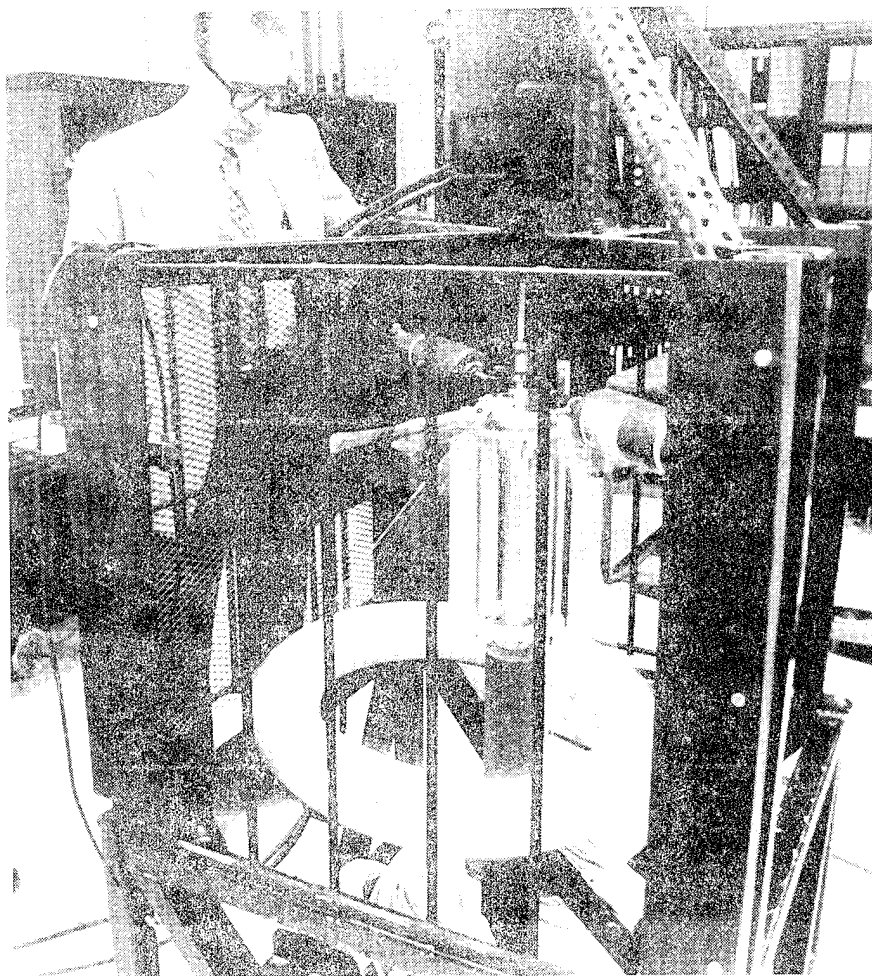
Fig. 2.   Flexible Flywheel Without Lower Radial-Constraint Ropes
(Flywheel Shown in Subsynchronous Whirl Mode)

17

The advantages claimed for the flexible flywheel with proper support system are:

1. High strength fibers in pure tension with no bonding materials to create mismatch in elasticity or strength.

2. Self-balancing, due to a highly flexible rotor operating at super-critical speeds.

3. Simple construction promotes economical production. Newly developed fibers can be easily incorporated without expensive redevelopment of manufacturing techniques.

4. Unbonded fiber construction simplifies the safe containment of a rotor failure.

5. Large hoop diameters made possible by the simple construction allow low operating speeds and attendant reduced power losses.

FLEXIBLE FLYWHEEL DESIGN EQUATIONS AND CONSTRAINTS

Analysis has shown that to optimize energy density, a flywheel should be constructed of high strength materials to operate at high speeds. The maximum storage energy in a hoop flywheel is

$$E = \pi r P \text{ ft-lb}$$

$$\bar{E} = (.3768)(10^{-6})\pi RP \text{ KW-hrs} \tag{1}$$

where R - hoop mean radius, ft

P - cumulative strength of all hoop fibers, lb.

Notice that the material mass density does not appear in the equation. Materials with high mass density (heavy materials) do not optimize energy density, which is contrary to popular intuition.

The mass density does, however, affect the speed at which the maximum energy is stored. This speed is given by

18

$$N_E = \frac{60}{2\pi} \sqrt{\frac{Pg}{\overline{w}R^2}} \quad \text{rpm} \qquad (2)$$

where $\overline{w}$ = hoop specific weight, lb/ft
g = 32.2 ft/sec^2

Although there are many advantages to using super-strong fibers to take advantage of equation (1), the resulting high rotational speeds (most high-strength fibers are not heavy) pose rotor dynamics and bearings problems which must be properly appreciated in the preliminary design phases of any modern flywheel. For example, contemporary electrical motors and generators are designed to operate well below the speed dictated by equation (2) for a Kevlar^R wheel.

There are also practical constraints on the dimensions of the flywheel to be used in the home or on a small farm. Figure 3 gives dimension limits for a fiber hoop flywheel.

Applying the above equations and constraints to the design of a flexible flywheel allows the calculation of hoop sizes, weights and costs for various choices of material. Comparative results for Dacron^R, steel, and Kevlar^R are shown in Table 1, for a 6 ft. diameter 10 KWh flywheel. Values for a 6 ft. diameter 50 KWh wheel are given in Table 4, page 59.

For a successful energy storage system, reasonable cost is essential. Table 1 shows that the high strength of Kevlar^R pays off in a lower total material cost for the flywheel. The technical price, however, is high operating speeds. It will be shown in the next section that the speed can also be brought down by the use of a larger hoop diameter. There are many applications, however, where space is limited and Figure 3 or similar constraints will govern the design.

19

Table 1. Parametric Values for a 6 ft. Diameter 10 KWh Flexible Flywheel
(Safety Factor = 2)

MATERIAL	HOOP WEIGHT lbs.	MAX. RPM	LENGTH L ft.	MAT'L COST $
Dacron (1/4")	1298	5,167	1.74	2954
Steel (1/2"IRWC)	2123	4,039	.642	1938
Kevlar (1500 Den.-"29")	162	14,606	.287	1280
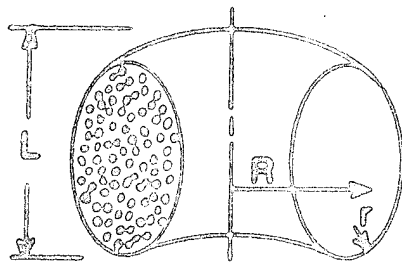
$R \leq 3$ ft.

$r \leq 4$ in.

$L \leq 4$ ft.

Fig. 3 Dimension Constraints

THE EFFECT OF SIZE

There are significant advantages to increasing the hoop diameter of a flexible flywheel.

The values in Table 1 were calculated under the constraints of Figure 3. If we choose Kevlar^R as the material, remove the constraint on the hoop radius "R", and again use a safety factor of 2, equations (1) and (2) can be written as

$$E = (10.97)R \text{ KWh} \tag{1}'$$

and

$$N_E = 31,005/R \text{ rpm} \tag{2}'$$

These equations show that the energy stored is increased and operating speed is decreased by making the hoop diameter larger (with constant circular cross section). Reference 4 shows that the latter effect (lower speed) reduces power losses.

Thus, a 10' diameter Kevlar^R flexible flywheel could store 50 KWh at a speed of only 6200 rpm, and have bearing power losses of only 178 watts. (See Appendix A for power loss calculation method.)

Furthermore, a flexible flywheel of large diameter can be constructed without the problems which would be expected from composite construction (inhomogeneous curing, uncertain shape and balance retention, high cost of manufacture, etc.).

ROTOR DYNAMICS

It was recognized early that the significant technical problems associated with the flexible flywheel would be in the area of rotor dynamics, specifically the problem of subsynchronous whirling due to internal friction. The advantage of self-balanced operation at high supercritical speeds must be purchased with the price of suppressing or avoiding a self-excited dynamic instability. This

is a challenge with a high payoff for success, and one which the author believes has been met.

Ever since Jeffcott's analysis of synchronous rotor whirl in 1919, rotor dynamicists have known that a flexible rotor displays a "critical speed inversion", in which the center of mass comes inside the whirling rotor center at supercritical speeds.

The flexible flywheel, by virtue of its low stiffness rotor, always operates at speeds which are highly supercritical, where Jeffcott showed that synchronous whirl (due to unbalance) amplitudes are minimized. Experiments to date have verified that the flexible flywheel produces extremely low levels of synchronous vibration, with no precision balancing required.

Not long after Jeffcott's results became widely known and applied, it was learned that rotating machinery can become dynamically unstable in subsynchronous whirl at supercritical speeds, if the ratio of internal friction (in rotating parts) to external damping is high enough.

Early tests of the flexible flywheel showed subsynchronous whirling which tended to grow with speed and/or time. Figure 4 illustrates the mechanism of the internal friction excitation. For subsynchronous whirl, the spin speed Ω is faster than the whirl speed ϕ. As support rope 3 moves around to position 1, its _rate_ of strain is a maximum at position 2, thus generating the friction force F or the hoop which is tangential to the whirl orbit in the forward direction.

Rotor dynamics theory and analysis has identified several ways of suppressing self-excited subsynchronous whirl. They are:

1. Flexible bearing supports.

2. Asymmetric bearing support stiffness.

3. Bearing support damping.

4. Bearing support mass (dynamic absorber effect).

22
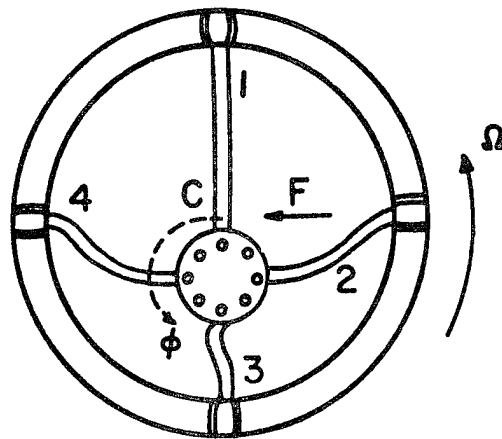
Fig. 4.   Instantaneous Configuration of Rope Ring

Before describing how these methods were applied to stabilizing a flexible flywheel, it is useful to take a preliminary look at the other "system" design considerations. A more detailed system design and cost analysis is presented in the last section.

PRELIMINARY SYSTEM DESIGN CONSIDERATIONS

1.   A shaft seal through the vacuum chamber wall is expensive.

2.   A disconnect clutch also increases the total system cost.

3.   A new motor/generator must be developed to match flywheel torque-speed characteristics.

4.   Low friction bearings must be designed for the application, to operate in a vacuum environment.

5.   The total number of bearings should be minimized, for lowest cost, and for lowest power loss.

When these design considerations are coupled with the design requirements to suppress the subsynchronous whirl, a design philosophy for the flexible fly-wheel emerges. The basic elements of this philosophy are shown in Table 2.

Table 2. Flexible Flywheel Design Philosophy

Design Factors or Constraints	Solution or Conclusion
Shaft seal is expensive New motor/generator required	Put motor inside vacuum chamber
Clutch increases cost New bearings required Minimize no. of bearings	Support flywheel directly from motor shaft
Need low support stiffness Need asymmetric support stiffness Need support damping and mass	Gimbal motor/generator on nonintersecting axes.

THE GIMBALLED SUPPORT DESIGN AND EXPERIMENTAL RESULTS OF WHIRL STABILITY

Figure 5 shows how the motor/generator can be gimballed on nonintersecting axes to provide the low support stiffness, stiffness asymmetry, and bearing support mass (the motor itself), which are the parameters important to whirl stability.

The motor bearings are designed to support the flywheel, thus minimizing the number of bearings and eliminating the necessity for a clutch, since the motor armature becomes effectively a part of the flywheel inertia.

Work on this contract has been aimed at verifying whirl stability for this concept, both experimentally and analytically. This section describes the experimental work; analysis is described in the section following.

24
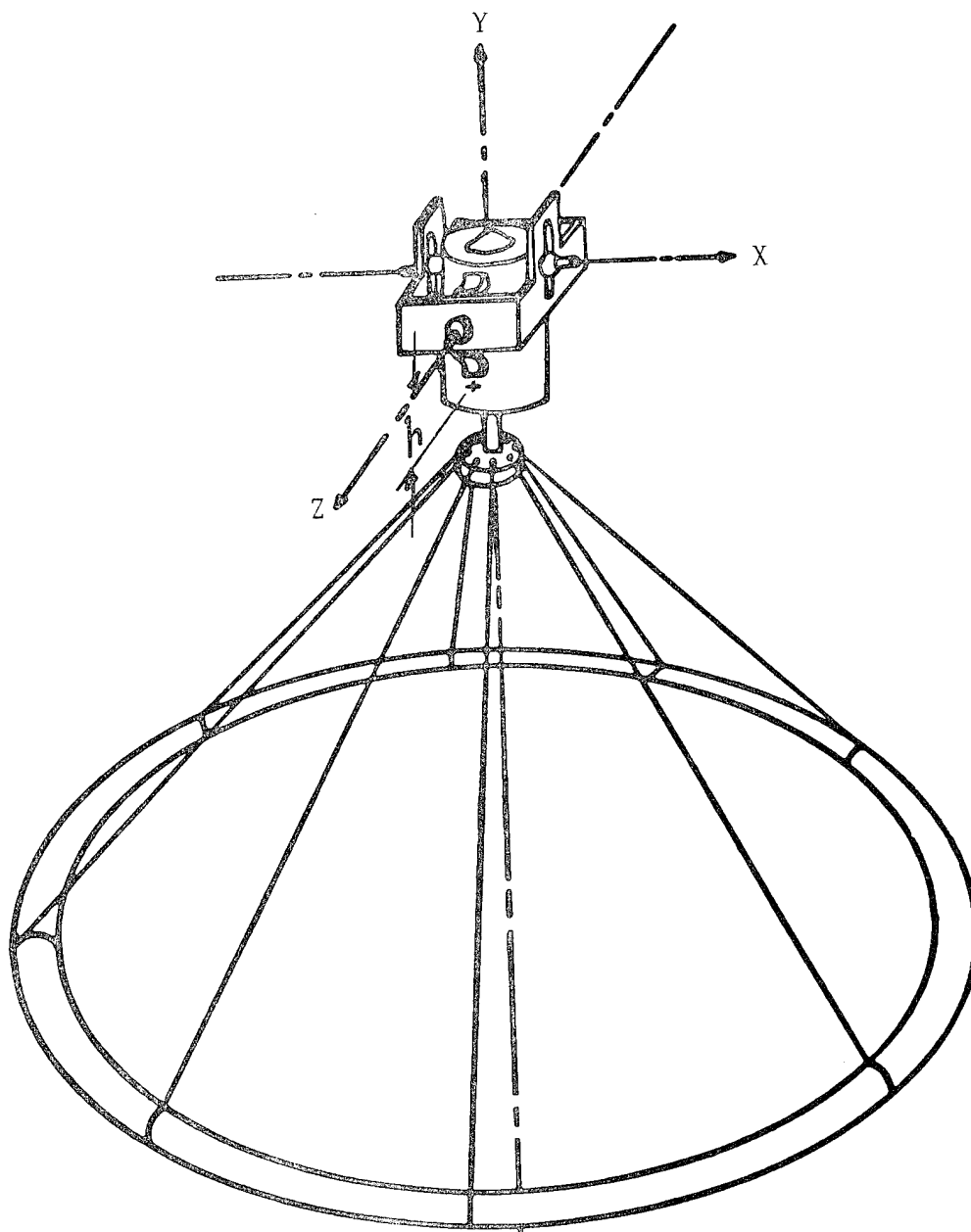
Fig. 5 Flexible Flywheel On Gimballed Support

A small scale model was constructed for preliminary evaluation of whirl stability characteristics. The distance h from the Z axis down to the motor center of mass was made adjustable, so as to vary the stiffness asymmetry produced by the gimbals. The flywheel used in this model is 10 1/2" diameter

and is made from a continuous coil of Nylon rope. The weight of the flywheel hoop alone is 2.7 lb. Figures 6 and 7 are photographs of the small model.

Tests were made with the gimbals locked (rigid), and with the gimbals free, to evaluate the effect on whirl stability.

With locked gimbals, the small flywheel is violently unstable in subsynchronous whirl at all speeds above 100 rpm, for all support rope configurations.

With the gimbals free, and twisted "maypole" support ropes, the flywheel is stable and runs smoothly up to the maximum speed allowed by available motor power to overcome air drag (about 2600 rpm). With the gimbals free and untwisted support ropes, the threshold speed of instability is between 600-750 rpm, depending on the length of the support ropes. In this configuration, asymmetry of the gimbal supports (one gimbal axis free, one locked) produces a slightly higher threshold speed than with both gimbals free.

No effort has ever been made to balance this flywheel, and at one time small unbalance weights were added at random to the twisted rope configuration to demonstrate its insensitivity to unbalance. The smooth and stable operation was not impaired.

A larger gimbal-supported motor/generator system was used to test a 22-1/2" diameter Dacron flywheel weighing 19 lb. Its 15 HP motor allowed speeds in the atmosphere up to 2000 rpm before air drag caused power supply circuit breakers to trip.

Figures 8, 9, and 10 show the 22-1/2" wheel with its motor/generator, gimbal support system, and protective cage.

The major shortcoming of the 22-1/2" wheel was its relatively low weight (19 lb.) compared to the motor/generator weight (90 lb.). It was felt that this impeded the stabilizing influence of the gimbals, an intuition which was

26
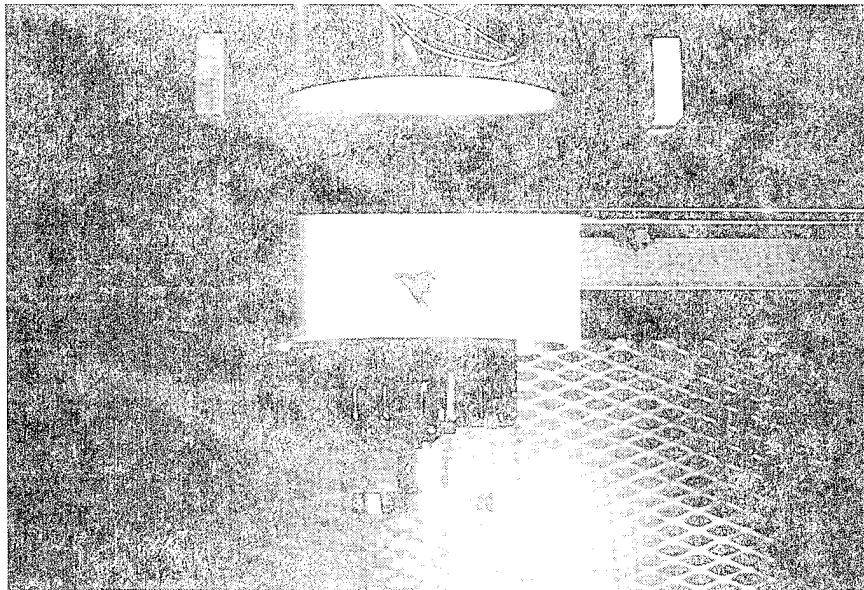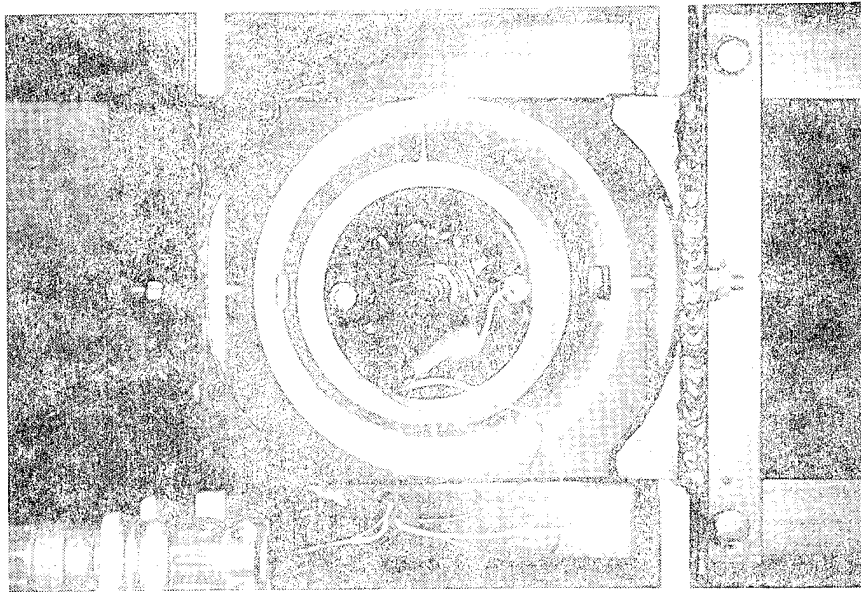
Fig. 6. Gimballed Motor For Small Model (10-1/2") Flywheel, Top
         and Side Views

27
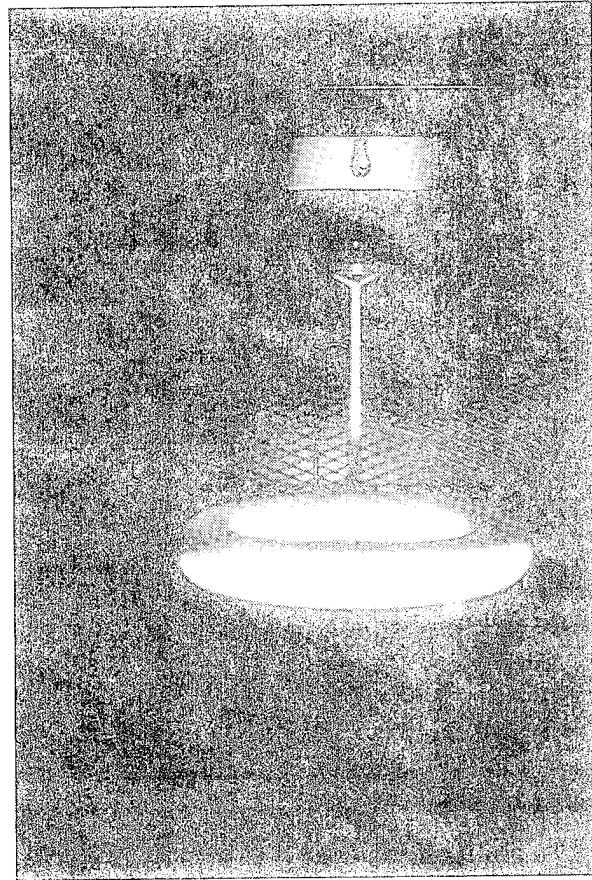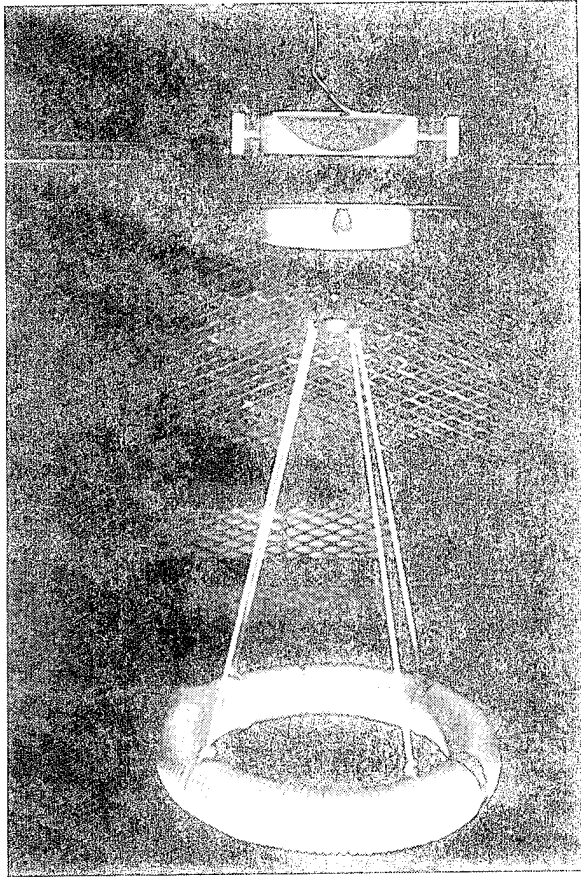
Fig. 7.   Small Model (10-1/2") Flywheel, With Untwisted Support
Ropes (left) and Twisted "Maypole" Support Ropes (right)
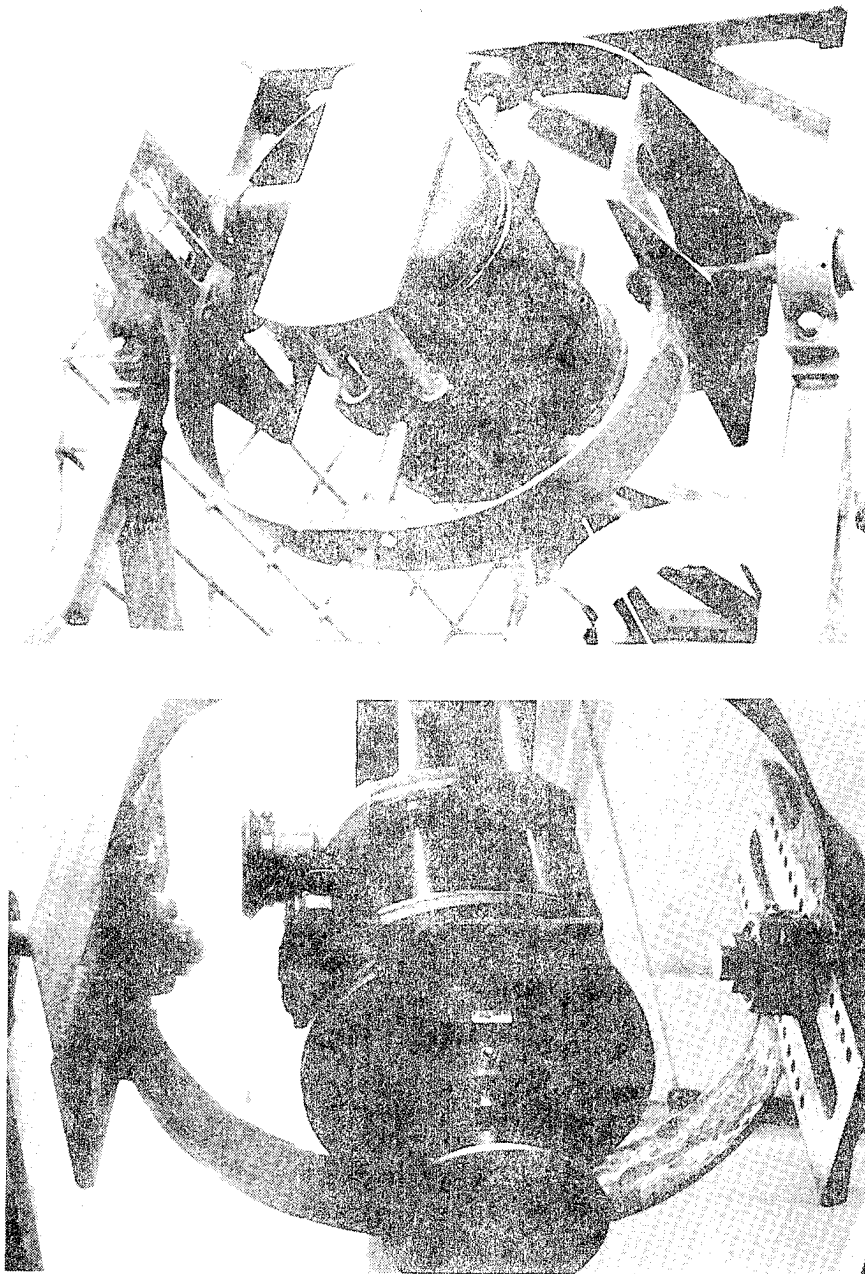
Fig. 8. Gimballed Motor and Cage for 22-1/2" Flywheel, Top and Bottom View
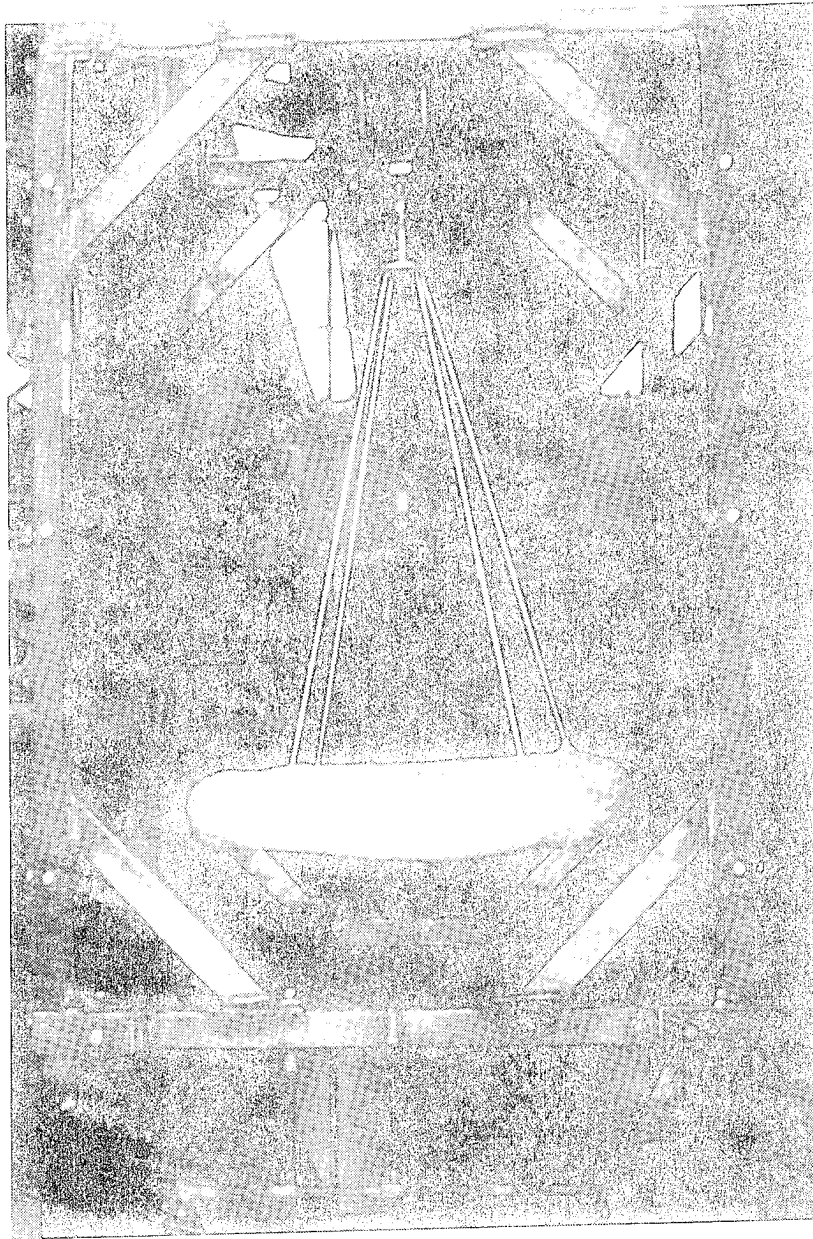
Fig. 9. 22-1/2" Flywheel on Untwisted Support Ropes
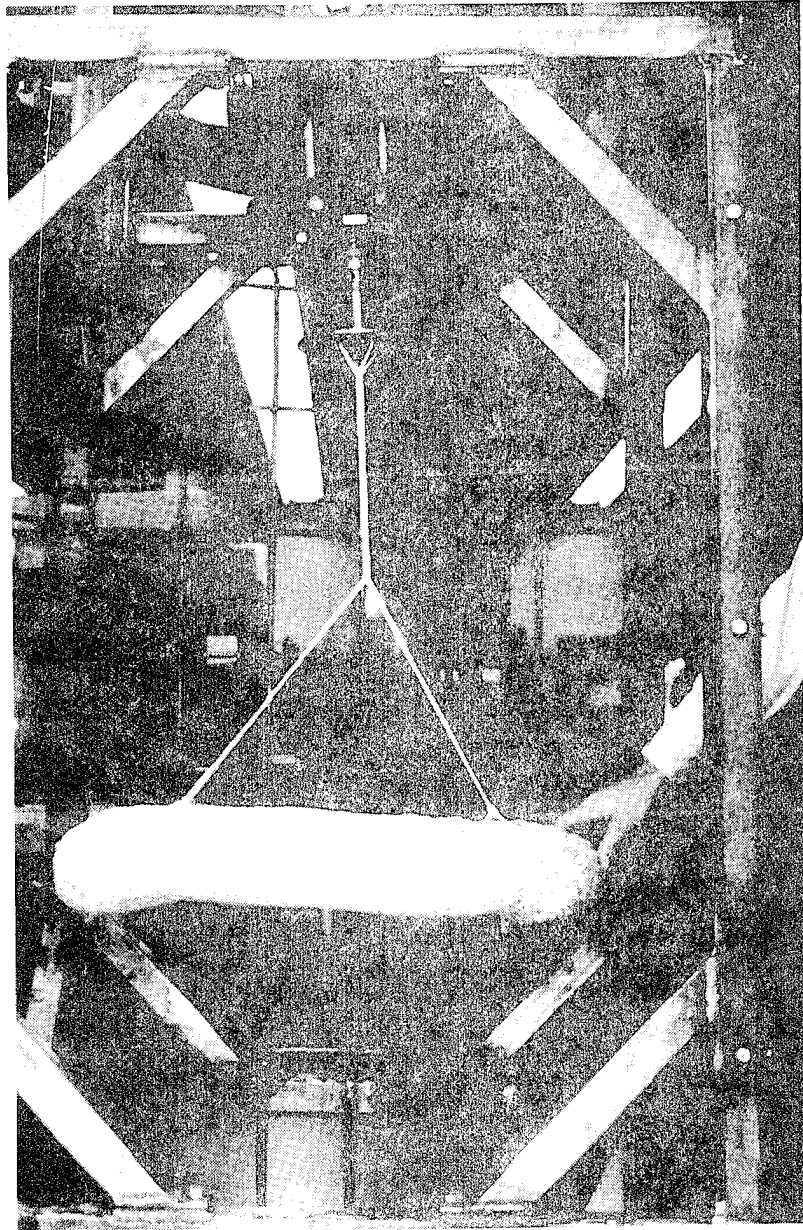
Fig. 10. 22-1/2" Flywheel on Twisted ("Maypole") Support Ropes

later verified by results from the computer stability analysis. Experiments with the 22-1/2" wheel showed an even stronger sensitivity to the method of support rope attachment, both at the flywheel and at the motor hub. The 2,000 rpm speed was achieved with untwisted steel cable supports attached to the fly-wheel with rope bridles. As mentioned above, the speed limitation in this case was imposed by excessive current demand tripping circuit breakers in the power supply. Shortly after this test, the 22-1/2" wheel was removed so that the motor/generator and gimbal supports could be installed in a vacuum chamber (as a safety measure, and for possible pump-down at a later date). After this was done, the 22-1/2" wheel was reinstalled, but the 2,000 rpm speed could not be repeated with untwisted support ropes. Since a considerable volume of air blows out of one of the chamber ports when the flywheel runs, it is felt that aerodynamic pressure may produce an additional destabilizing force in the chamber. Another possibility is that the support cable attachment scheme was not precisely duplicated after reinstallation.

Finally, a 30" diameter Nylon wheel weighing 88 lb. was constructed and tested in the vacuum chamber, using the 15 HP motor/gimbal assembly shown in Figure 8. This flywheel can store 1 KW-hr at 10,650 rpm, and has a breaking speed of 14,548 rpm. Figure 11 shows the vacuum chamber, and Figure 12 is a photograph of the 30" flywheel in the vacuum chamber (looking down from the top). With the flywheel supported by untwisted support ropes made from monofilament Nylon, the threshold speed of instability was 1,000 rpm. To simulate the twisted "maypole" support ropes which had proved stable in the smaller models, and yet retain torque capability in both directions, a four strand bridle was braided into a square cross section. With this support rope configuration, the maximum speed achieved was 1500 rpm and was limited only by the power supply overload due to air drag.

32

Fig. 11. Vacuum Chamber for 30" Flywheel

Fig. 12. 30" Flywheel Installed in Vacuum Chamber

TORQUE AND POWER CAPABILITY OF THE SUPPORT ROPES

To answer questions raised about the ability of the support ropes to transmit sufficient torque for generating useful magnitudes of electrical power, the torque actually transmitted in overcoming air drag on the 22 1/2" flywheel was measured. This was accomplished by measuring the rope angles in photographs and movies, and relating these angles to static torque measurements. The results, converted to KW at various speeds, are shown on Figure 13. It can be seen that the twisted rope configuration (previous Figure 10), the one of primary interest, would generate over 1.3 KW at 6,000 rpm and over 2.2 KW at 10,000 rpm. It can be assumed that this torque/power transmitting capability will increase with the flywheel diameter and with the moment of inertia of the cross-section area of the quill shaft which is created by the twisted support ropes. This assumption is supported by torque tests on the 30 inch diameter nylon flywheel in which four 1/4 inch support ropes (same size ropes as used on the 22 1/2 inch diameter flywheel) were square-braided to form a quill shaft with a cross-section area of greater moment of inertia than was obtainable by "maypoling" the ropes into a shaft of essentially circular cross-section. The input power required for the motor to drive this 30 inch diameter flywheel at 1500 rpm in the atmosphere translates into approximately 6 KW power generating capability in a vacuum.

INSTRUMENTATION AND MEASUREMENTS

Flywheel speed of the small (10-1/2") model was measured with a photocell reflective tachometer. The reflective tape was installed on the flywheel hoop itself. Natural frequencies were measured with a SELSPOT optical tracking instrument, tracking the motion of LED's installed on the flywheel. The signal was captured on a storage oscilloscope, so that the logarithmic decrement
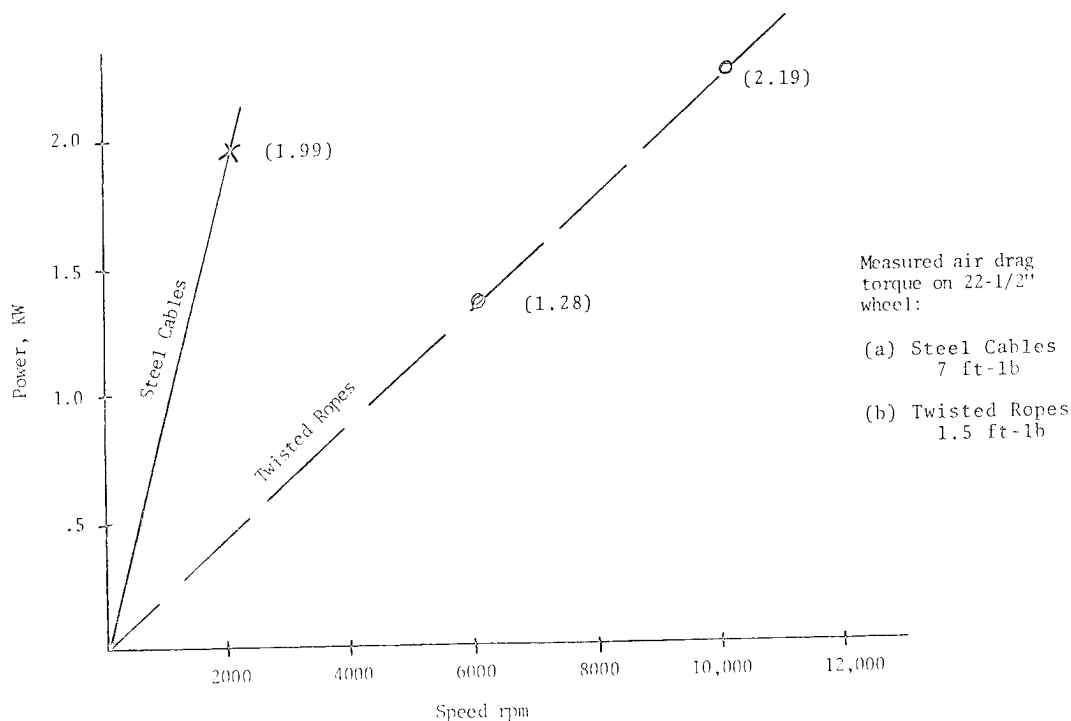
Fig. 13. Electrical Power Capability of Flexible Flywheel From Measured Torque

(damping) could be determined as well as the natural frequency.

Flywheel speeds of the larger (22-1/2" and 30") flywheels were measured with a pulse tachometer, consisting of a magnetic transducer excited once per revolution by a projection from the steel hub of the motor shaft, with the period between pulses measured by an H-P electronic timer. (An electronic tachometer reading in rpm was also used in the early stages of the project).

Whirling frequencies of instability were so low (typically 1-2 Hz) that it was found possible to measure them visually, using a stopwatch, and by movies, placing a clock with a sweep second hand in the camera field of view.

Due to the flexible support with no hub or spokes, the flywheel hoop whirled as a rigid body. No flexural vibrations of the hoop (as envisioned in the original proposal for this contract) were ever observed.

36

FLEXIBLE FLYWHEEL STABILITY ANALYSIS

I. The Mathematical Model

A mathematical stability analysis was performed on the flexible fly-
wheel so that its stability characteristics can be predicted for any given
set of system parameters. In particular, it is desirable to know which
parameters have the most pronounced effect on the system stability when they
are changed. Three different mathematical models were considered and actual
computer simulation was performed for two of them. The most important dif-
ference between the three models is the configuration of the support ropes
which join the flywheel to the gimballed motor.

A. Rigid shaft model

The first model to be considered is shown in Figure 14. The gimballed
support system has been modeled to allow for the rotation of the motor about
the gimbal axes in the presence of viscous damping. All mass properties of
the motor and its support system have been taken into account, including the
gyroscopic effects of the motor's rotating parts. The flywheel itself is
modeled as a rigid rotor with all its corresponding mass properties, including
gyroscopics. External damping on the flywheel is assumed to be viscous air
drag proportional to the flywheel's translational velocity and acts at the
flywheel's center of mass.

The most important aspect of this model is the modeling of the support
ropes. The support ropes are assumed to be straight and to remain straight
at all operating speeds. This would result in the ropes behaving collective-
ly as a rigid shaft attached rigidly to the flywheel and flexibly to the
motor. With the ropes modeled as such, the internal friction force due to
hysteresis in the ropes will then be proportional to the misalignment angle
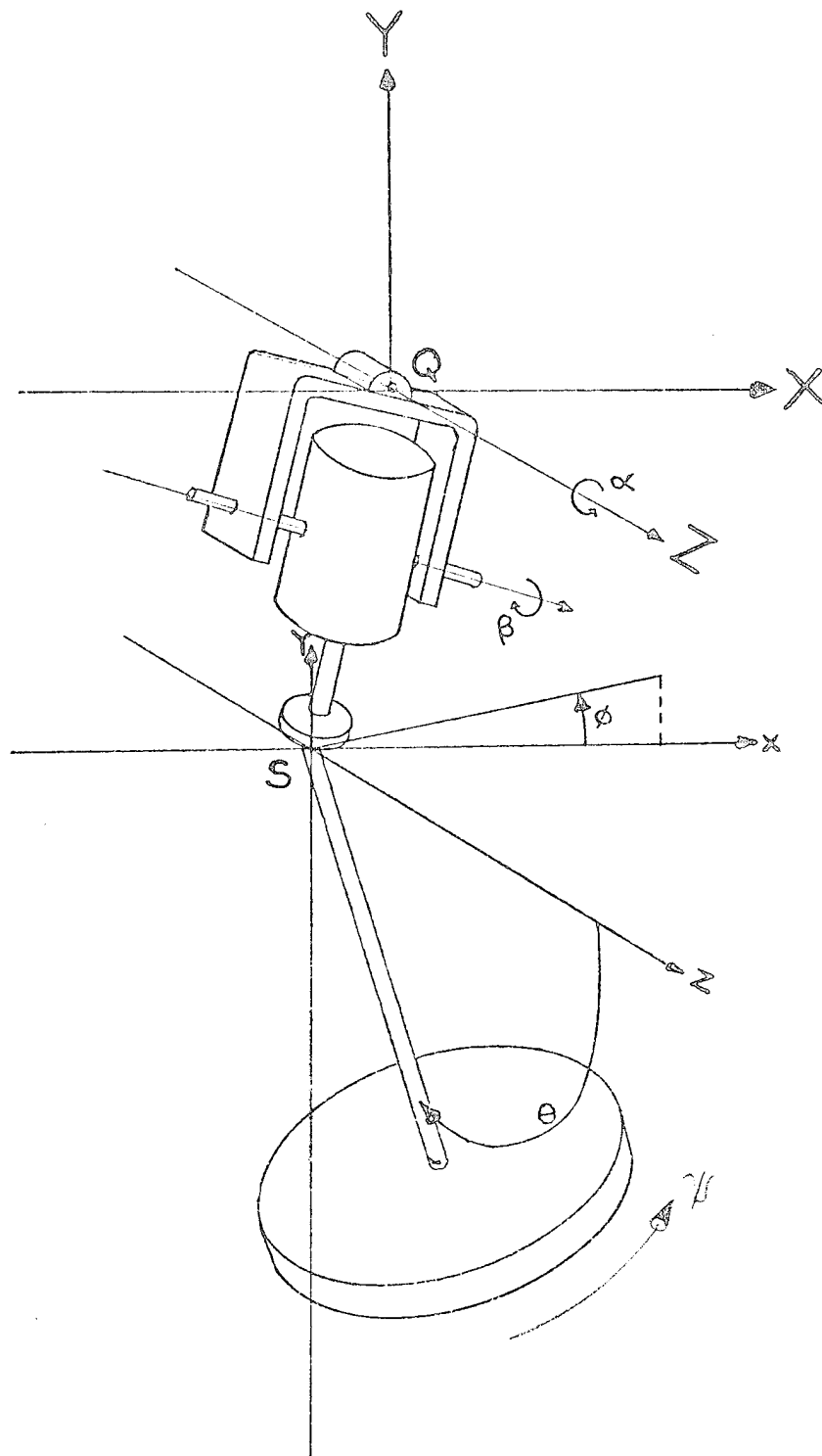
Fig. 14. Flexible Flywheel Model With "Rigid-Shaft" Support
Ropes and Gimballed Motor/Generator

between the motor's main axis and the rigid shaft that makes up the support ropes.

The model just described has five degrees of freedom. Two angles α and β have been used to describe the motor's orientation, each angle being the rotation about one of the gimbal axes. Three more angles, ϕ, θ and ψ are used to specify the flywheel's orientation. One of these flywheel angles, ψ, constitutes the spin of the flywheel, and by assuming the flywheel's acceleration to be small, constant speed can be assumed to reduce the system to four degrees of freedom.

Since the model has four degrees of freedom, the system will have four natural frequencies and four corresponding mode shapes. Each mode shape is, in fact, a whirling configuration with both the flywheel and the motor executing a circular or elliptical path. Two of these modes will have the flywheel executing a rather large motion with the motor following along with it. One of these will be a forward whirl in the direction of flywheel rotation and one will be backwards whirl. The two remaining mode shapes occur at the critical speeds of the motor support system. In these modes the motor will execute the large motion and the flywheel will remain relatively stationary. Once again, one mode will be forward whirl and the other will be backwards.

The four second order differential equations of motion for this system have been derived using Lagrange's method and are given in Appendix B.

B. Bowed-out rope model

When the flywheel is spinning at a high speed, the support ropes no longer remain straight but will bow outwards due to the centrifugal forces acting on them, see Figure 15. With the support ropes in this bowed-out configuration, they no longer act like a rigid shaft, rigidly connected to the flywheel as was

39
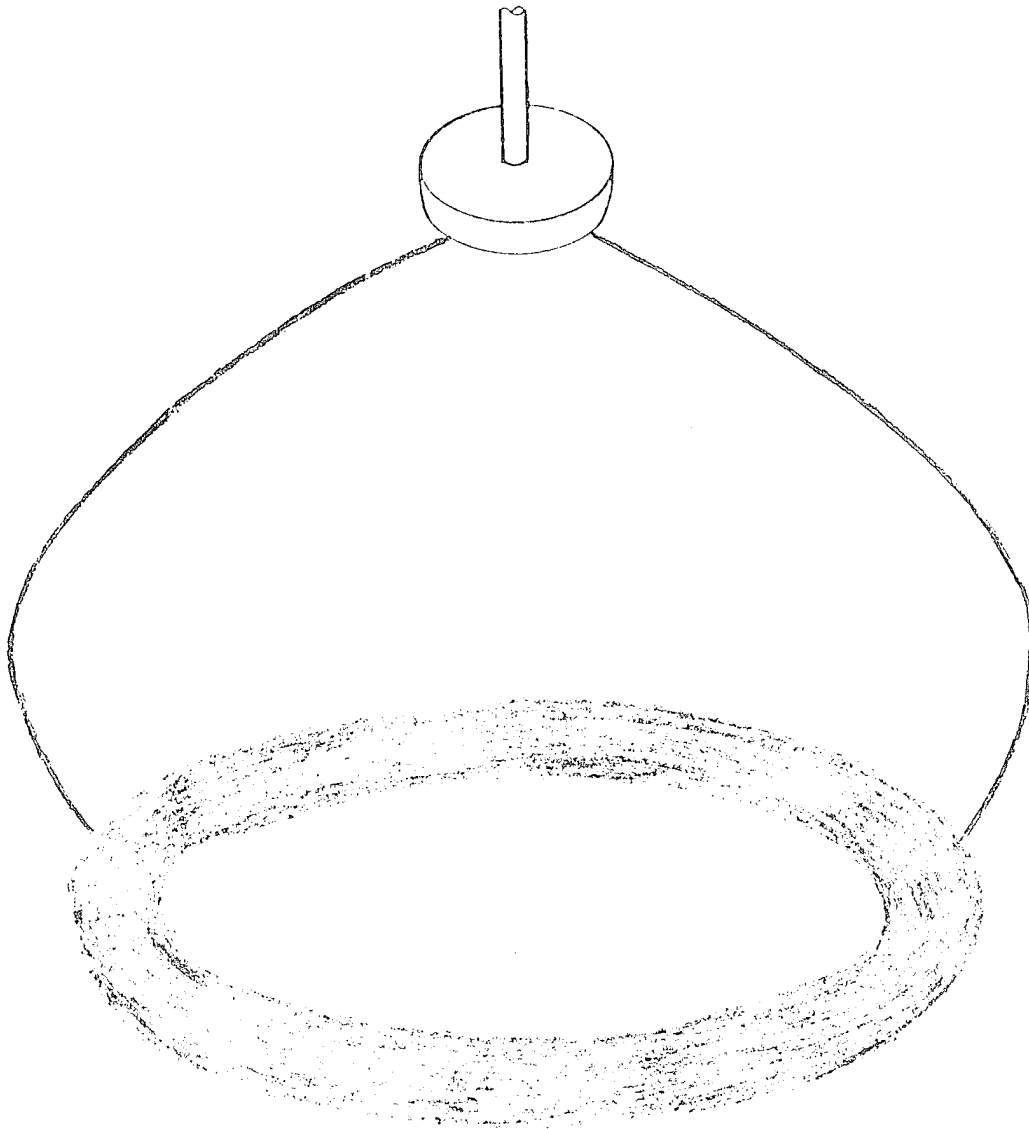
Fig. 15. Flexible Flywheel Model With "Bowed-Out" Support Ropes

assumed in the first model. This additional flexibility provided by the bowed-out ropes allows the flywheel to take on any orientation independent of its position.

When the flywheel is spinning at a high speed, the gyroscopic moments tending to keep the flywheel horizontal are very strong. This gyroscopic effect tends to keep the flywheel horizontal, even when it is in a whirling configuration. This causes the internal friction forces to act differently than in the rigid shaft mode. The internal friction force in each rope is proportional to the rate of strain which in turn is determined by the geometry of the system and the speed of the flywheel. But, since the geometry is now different, then so will be the internal friction force at any given speed.

Taking into account the new geometry of the system, new differential equations of motion were derived again using Lagrange's method, see Appendix B. The same angular coordinates were used as for the rigid shaft model, and are analogous to their counterparts for the rigid shaft model.

C. Twisted rope model

The third model considered is essentially the same as the first two models. The main difference is that the support ropes are now twisted around them- selves, see Figure 16. This twisting of the ropes causes a considerable change in the stability of the system, as is observed with the small (10-1/2") model flywheel.

For this twisted rope system the differential equations of motion were not derived and a computer analysis was not performed. However, a theory has been developed to explain the observed behavior of the twisted rope system. (Both its stability with the gimballed motor and its instability with the rigidly supported motor.)
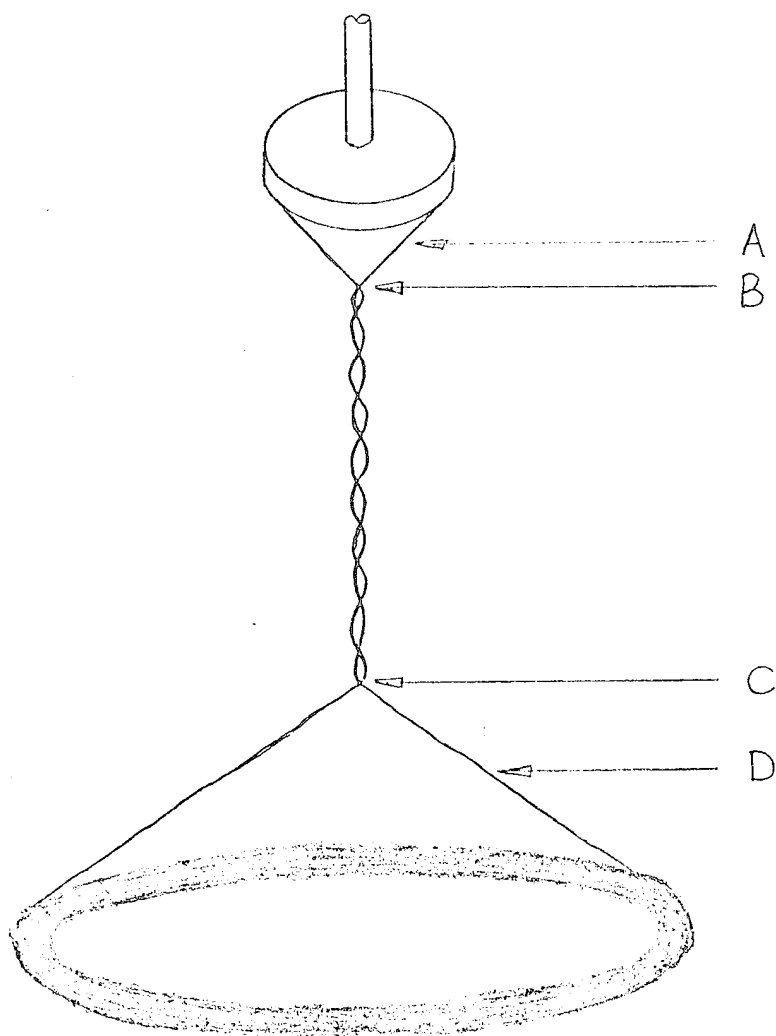
Fig. 16. Flexible Flywheel Model on Twisted Support Ropes

When the support ropes are twisted and the flywheel is in a whirling configuration, see fig 16, gyroscopic moments will keep the flywheel horizontal as with the bowed-out rope model. This produces internal friction forces in four different regions of the support ropes, labeled A, B, C and D in the figure. In regions A and D, the internal friction forces are produced in exactly the same manner as for the rigid shaft model and thus will be in the direction of forward whirl. In region B the internal friction force is produced in much the same manner as in a spline fit coupling. It will therefore be in the direction of forward whirl and it will be equal to zero when the twisted ropes are in line with the motor. The internal friction forces produced in region C are produced in the same way as for region B except that now it will be in the direction of backwards whirl.

When the rotating flywheel is in a whirling configuration with the motor held rigid, the forces produced in regions B and C will be equal and opposite and thus will cancel. The forces produced in regions A and D will both be trying to produce forward whirl, and thus the flywheel should be expected to go unstable at a rather low speed. This prediction matches exactly the behavior observed for the small (10-1/2") model flywheel.

When the motor is allowed to rotate in its gimballed support, and the flywheel is in a whirling configuration, the motor will follow the flywheel around so that the motor axis is always in line with the twisted ropes. This action will cause the friction forces in regions A and B to both be zero. The friction force in region C will still be in the direction of backwards whirl, and in region D it will be forward. Thus, the only internal friction forces present will be acting against each other. There is no reason to suspect that they will be equal and opposite, but the resultant can be expected to be much smaller than in the case of the rigid shaft model or the bowed-out ropes model. It also should be possible to somehow adjust the

43

two forces so that they are equal and opposite, resulting in no net internal friction force and stable operation at all speeds.

The small model flywheel is seen to be stable at all speeds of operation when the support ropes are twisted and the motor free, and so the predictions based on the theory just presented match exactly its observed behavior. If this theory should prove to be correct, then the internal friction instability can be eliminated even if the flywheel is operated in a vacuum without the stabilizing effect of air drag.

II. Internal Friction Force

In both the rigid shaft model and the bowed-out ropes model, the internal friction force is generated in the same manner by hysteresis in the support ropes. The magnitude and direction of the internal friction force is dependent upon the displacement of the system although this dependence is entirely different for the two models. The qualitative relationship between the system displacement and the direction of the internal friction force will now be considered for the two models.

A. Rigid shaft model

For this model, the internal friction force is proportional to any misalignment between the motor and the flywheel. The internal friction force will be zero only if the axis of rotation of the flywheel is colinear with the axis of rotation of the motor. Figures 17a and 17b show, in a simple way, all the possible configurations that the system can assume. The motor is shown in an arbitrarily deflected position and the flywheel can be anywhere on the indicated curve for the given motor deflection. Depending on where the flywheel is on this curve, the friction force may be in the direction of forward whirl or backward whirl. The various regions are also indicated on the figure.

44
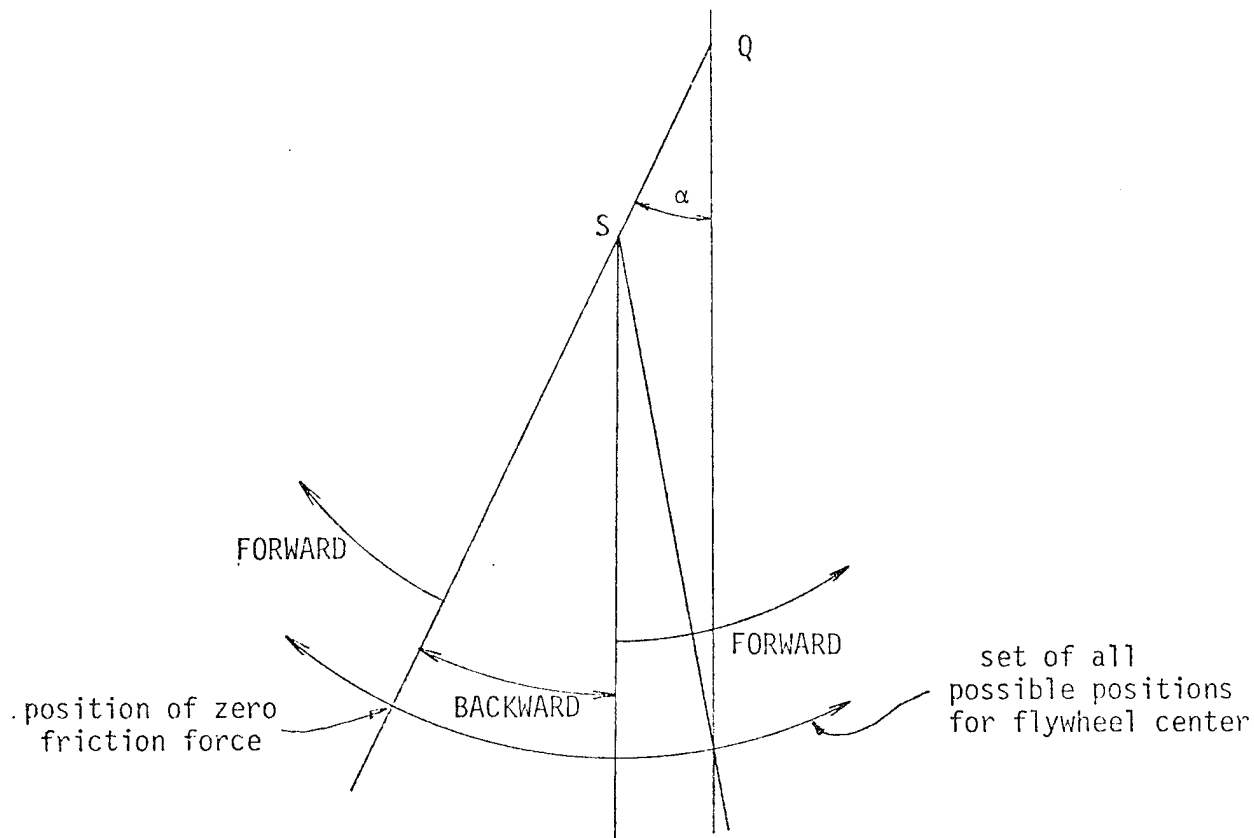
Fig. 17a.   Internal Friction Force For Model With "Rigid-Shaft"
            Support Ropes For Deflection About Upper Gimbal Axis

45
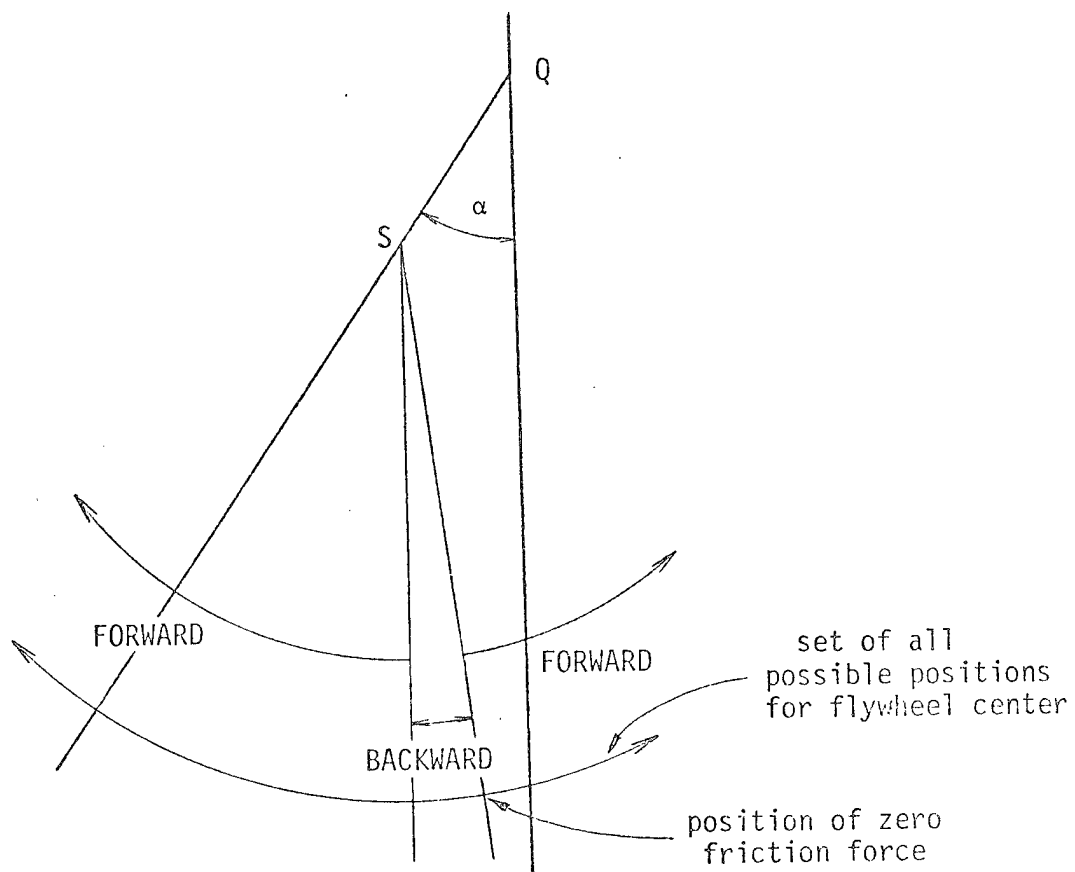
Fig. 17b. Internal Friction Force For Model With "Rigid Shaft"
Support Ropes For Deflection About Lower Gimbal Axis

If a mode shape which executes forward whirl should have the flywheel in a region labeled "forward" on the figure, then the internal friction force will be in the direction that the flywheel is trying to move. Under these circumstances, the system will stand a very good chance of going unstable. The same holds true if a backwards mode shape should happen to put the flywheel in a region labeled "backwards".

On the other hand, should a forward mode shape put the flywheel in a region labeled "backwards", then the flywheel would not be expected to go unstable since the internal friction force would be opposite the direction that the flywheel wants to go. A backwards mode shape in a "forward" region would produce the same effect.

Conceivably, it could be possible to find a special set of system parameters that will, for each mode shape, locate the flywheel in a region of opposing internal friction force. If this is done, then one can expect stable operation at any operating speed for a flywheel that actually is supported by a rigid shaft, or quill shaft.

B. Bowed-out rope model

For this model, the relationship between system deflection and the internal friction force is more complicated and depends on more system parameters. The two drawings in Figure 18 show the friction for the small (10-1/2") model flywheel. Figure 18a applies to forward-backward motion for deflection about the upper gimbal axis and Figure 18b to forward-backward motion about the lower gimbal axis. The reason for these separately defined motion planes (90 degrees apart) is that the gimbal axes do not intersect, thereby causing the geometric conditions to alternate as the flywheel whirls around. This, along with the dependence on more system parameters, makes it seem very possible to overcome the instability by varying the system parameters.
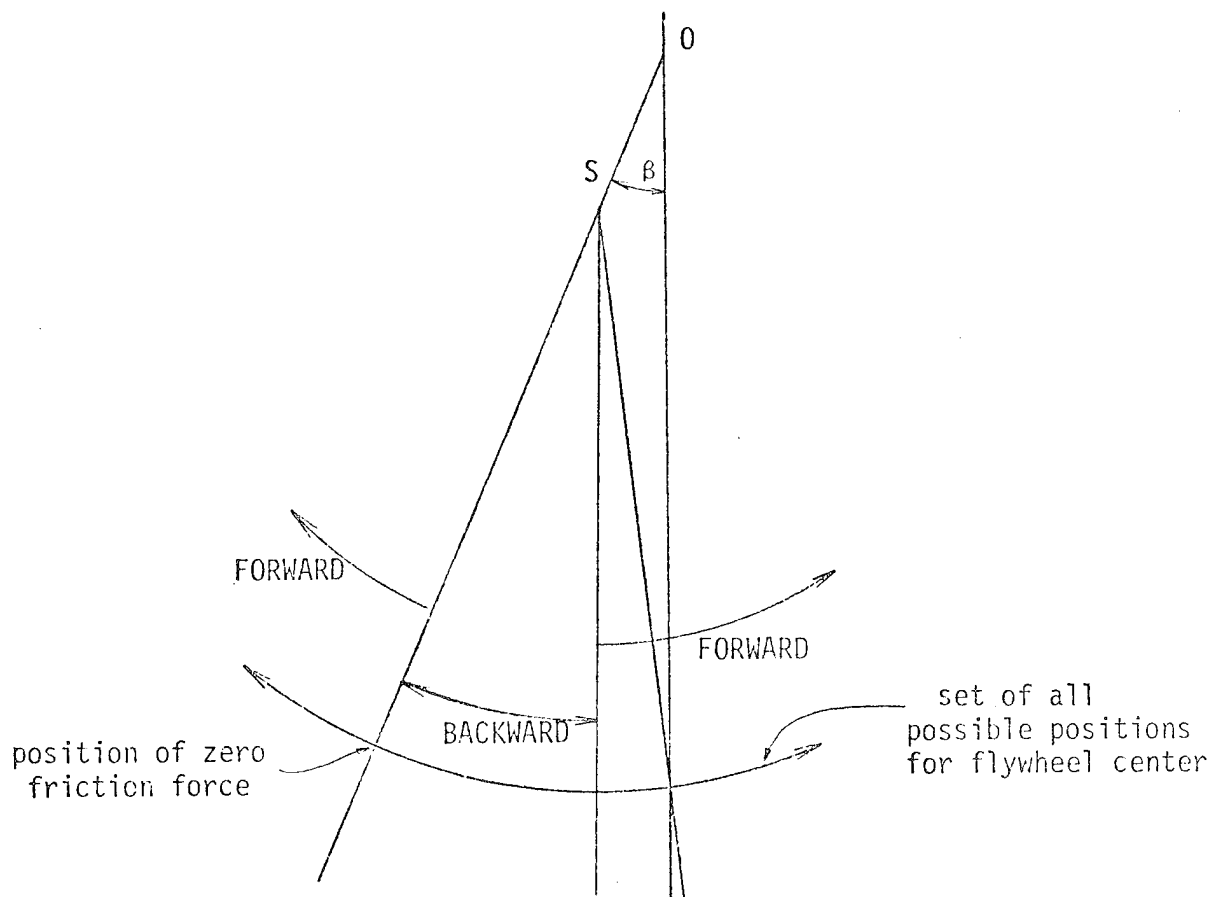
Fig. 18a. Internal Friction Force For Model With Bowed Ropes
For Deflection About Upper Gimbal Axis

The stability of the small (10 1/2") model flywheel has been observed
to be slightly enhanced by making the support ropes shorter. To illustrate
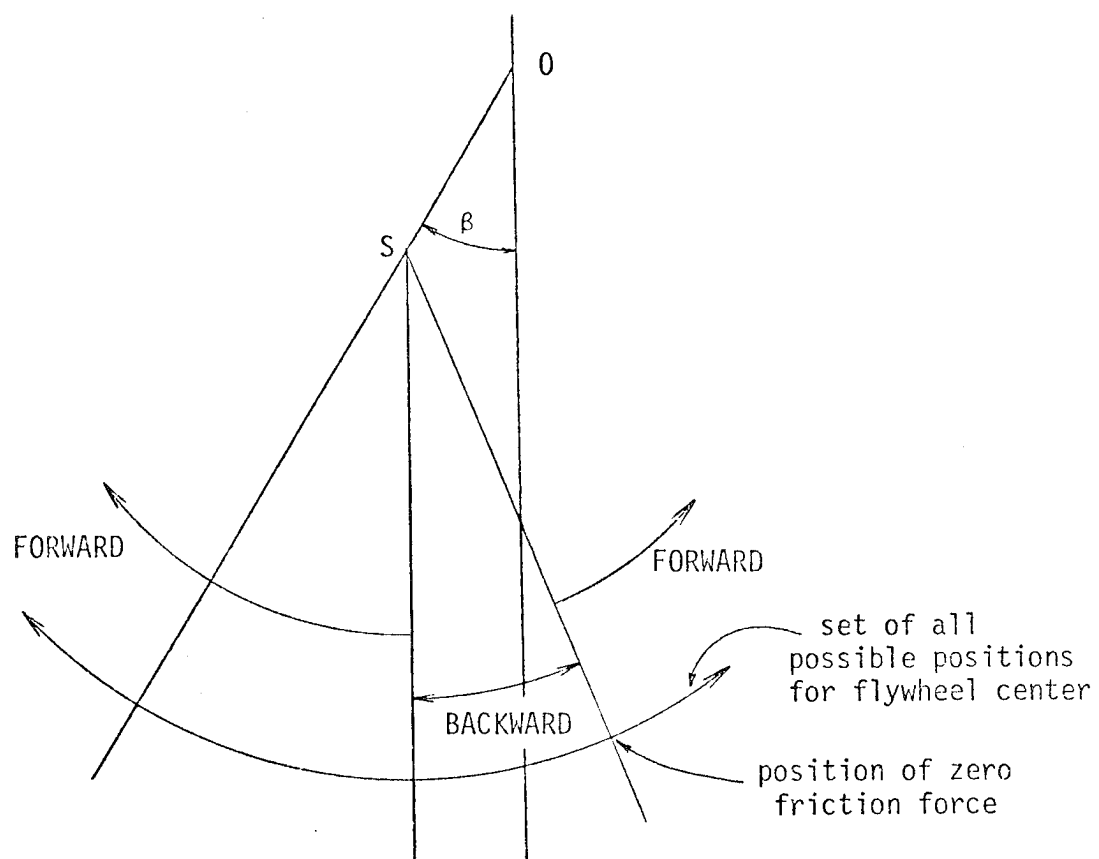
Fig. 18b. Internal Friction Force For Model With Bowed Ropes
For Deflection About Lower Gimbal Axis

49

how the mathematical analysis can be used to investigate this sort of behavior, the computer program was used to predict system stability for support ropes of various lengths. Figure 19 shows the results of this work and it can be seen that the threshold speed of stability does indeed increase when the support ropes are shortened. There is, however, a practical limit to how short the ropes can be made because synchronous vibration due to unbalance starts to increase rapidly as the ropes are made shorter.

III. Computer Solution

The differential equations of motions for the rigid shaft model and the bowed-out ropes model are given in Appendix B. These equations represent mathematical relationships between all the forces, external and internal, acting on the system and the resulting motion of the system which at this point is unknown. For each model, the equations form a linear, eighth-order system comprised of four, linear, second-order differential equations which are homogeneous and have constant coefficients. These equations can be solved to yield the general solution in terms of some unknown constants as follows.

First, the four, second-order equations can be converted to eight, first-order equations by the definition of four new coordinates which are equal to the velocities of the four existing coordinates. Substitution of these four new variables into the second-order equations eliminates the second-order terms and reduces the equations to first-order. This procedure yields eight, first-order equations which can be written in matrix form as

$$\dot{x} = [A]x \tag{1}$$

where x is the state vector describing the configuration of the system and $\dot{x}$ is the time derivative of x. The matrix A is the square matrix made up of

50
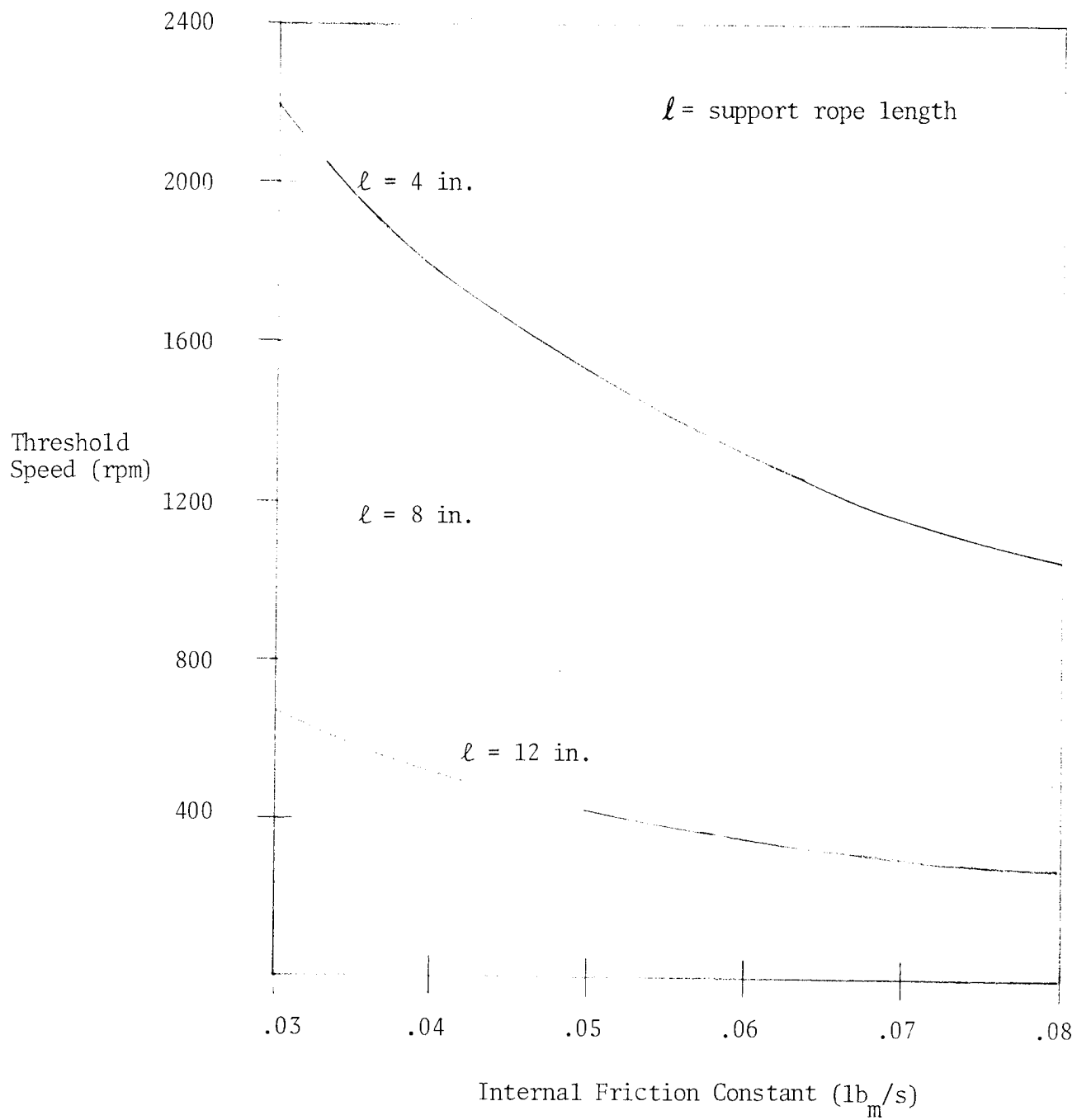
Fig. 19. Threshold Speed of Instability for 10-1/2" Flywheel

the coefficients of the four original equations. The solution to this matrix equation is known to be an exponential of the form

$$x = C\ e^{\lambda t} \tag{2}$$

where C is a vector the same rank as x, and λ is a constant known as an eigenvalue. In general, C and λ can both be complex having real and imaginary parts. Substituting (2) into (1) gives

$$\lambda Ce^{\lambda t} = [A]Ce^{\lambda t}$$

or
$$([A] - [I]\lambda)\ Ce^{\lambda t} = 0 \tag{3}$$

For this equation to have a non-zero solution, it is necessary that the matrix, defined by the expression within the parentheses, not be invertible. This requires that its determinant be equal to zero , or

$$\left| [A] - [I]\lambda \right| = 0$$

The determinant will be zero only for special values of λ, termed eigenvalues. The eigenvalues are obtained by expanding the determinant into a polynominal in λ, and then solving for the roots. In the case of the flywheel, the resulting polynomial will be eight-degree and will thus yield eight eigenvalues. In general, this eight-degree polynomial is impossible to solve analytically and so the computer is used to find the eigenvalues using a program outlined in Appendix C.

The eigenvalues contain some of the most important information about the system. For each particular mode of motion for the system, there is an eigenvalue that pertains to it. The imaginary part of the eigenvalue is the damped natural frequency for the particular mode. The real part of the eigenvalue is the damping exponent and it determines the stability of motion in the mode. If this damping exponent is a negative number, then any motion in this mode will decay with time and eventually die out so the system is stable. Should it be a positive number, then the motion will grow exponentially with time and the system is termed unstable.

52

In order to determine what shape the system takes on when there is motion in a particular mode (i.e., the mode shape), it is necessary to first find the eigenvector corresponding to the mode in question. The eigenvector is a complex vector that is obtained by taking an eigenvalue and substituting it into Equation (2) and solving the resulting system of linear algebraic equations for the complex constant C which will be the eigenvector. The actual mode shapes are then obtained directly from the eigenvectors by a procedure discussed in Appendix C.

CONCEPTUAL DESIGN AND COST ANALYSIS OF A 50 KWh FLEXIBLE FLYWHEEL ENERGY STORAGE SYSTEM

The performance requirements, which form the basis for this analysis, are that the flywheel interfaces with a small solar electric energy system for residential applications. In meeting this criteria, the flywheel must be sized to store a nominal 50 KWh of energy and the motor/generator must supply 10 KW peak power.

Definition of Components

Rotor: The rotor is comprised of a flexible flywheel which is inherently self-balancing. The flywheel is a simple hoop, constructed by coiling ropes, cables, or fibers in a circle of the desired radius until the design mass is achieved. In operation, centrifugal force maintains the circular configuration. To maintain shape integrity when not spinning, an outer sheath surrounds the cross section of the hoop. The hoop is suspended by flexible ropes which carry only the weight of the flywheel and provide a non-rigid connection between the rotor and the motor generator.

Bearings: The motor bearings provide support for the flywheel in addition to their normal functions in the motor. This design both minimized the number

53

of bearings in the system and eliminated the necessity for a clutch between the motor/generator and rotor. These bearings must be capable of high speed, low drag operation in order to minimize system losses.

Vacuum Vessel: In order to keep air drag losses down to acceptable levels, the rotor assembly must operate in a vacuum vessel capable of maintaining a vacuum of 10 microns or less. The vacuum vessel performs the the additional role of providing support assemblies from which the gimballed motor/generator and rotor are suspended.

Vacuum System: In order to maintain the vacuum vessel at or below 10 microns, two vacuum system options are available depending on the leak rate of the vessel. By designing the vessel with a low leak rate, only occasional evacuation would be required. This option envisions a mobile vacuum service periodically visiting the different sites and performing pump-down with on-board equipment as required. The second option is to have a vacuum system permanently attached to the vacuum vessel providing continuous evacuation. This option allows higher leak rates at the cost of energy to run the pumps.

Electronics: The electronics provide the interface between the motor/generator and input-output power requirements. On input the electronics must perform the task of maximum power tracking to allow efficient transfer of power from the solar array to the motor. On output the electronics system must accept the electrical energy from the generator and carry out the required power conditioning (DC to AC, voltage changes, etc.) to allow efficient use at the load.

Safety Devices: The flexible flywheel's gradual failure mode, unraveling allows for a minimum of safety devices. Sensors in the vacuum vessel can monitor for early warning signs such as hoop growth or whiplash and shut down the

flywheel system before final failure. Even if failure should occur, the rotor does not rapidly disintegrate due to its self-balancing characteristics. As such, safety devices need not be as rigorous and extensive as with solid rotors.

Oil cooling system: To provide cooling for the motor/generator, transformer oil is circulated around the motor windings. The system consists of a heat exchanger, oil pump and cooling lines to the motor generator. The cooling lines inside the vacuum vessel must be flexible to allow the gimbal action of the motor/generator.

Elements Defined By Technological Requirements

Three components of the flywheel system are defined by technological constraints. These elements are the rotor, the motor/generator, and the bearings. These requirements and their relationship to each component are given in Table 3.

A unique feature of the "flexible flywheel" is the construction of the rotor from flexible fibers (such as synthetic rope) with no bonding agents. The advantages of this configuration are:

1. Self balancing-highly flexible rotor operates at supercritical speeds.
2. Simple construction.
3. High strength fibers in pure tension with no bonding materials to create mismatch in elasticity or strength.
4. Gradual failure mode, with early warning by whiplash or hoop growth.

Figure 20 shows the basic design of the rotor hoop as well as some practical limits on the radii involved. The height (L) of the hoop is varied with each material in order to obtain the rotor's required mass. The practical limit on L is probably about four feet. A large L, however, introduces an additional

55

TABLE 3. Satisfaction of System Requirements

Technological Requirement	Component affected/ Solution for Problem
50 KWh storage capacity Self-balancing Gradual failure mode Failure early warning Hoop height less than 4' for stability	Flexible hoop rotor
High drag in rotary vacuum feed-through Gimballing action required at motor for stability	Motor/generator in vacuum
Need low support stiffness Need asymmetric support stiffness Need support damping and mass	Gimbal motor/generator on nonintersecting axis
Low drag High speed operation	Bearings
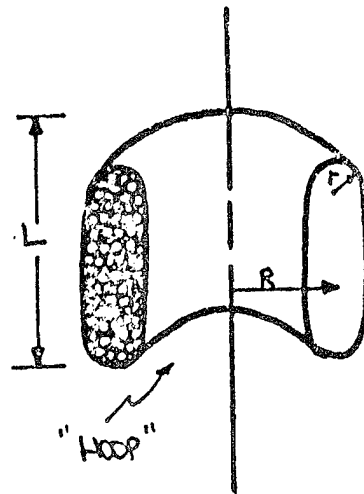
R = 3 ft.

r = 4 in.

L defined by material

Fig. 20.   Rotor Hoop Dimensions

dynamic whirl mode with its potential instability. Therefore, the height of the rotor should be kept within reasonable limits.

Possible materials for the construction of the rotor include Nylon, Dacron, high strength carbon steel cable, and Kevlar-29 fiber. A comparison of rotor hoops constructed of these materials can be found in Table 4. Based on keeping the rotor height to a minimum, one can quickly eliminate Nylon and Dacron from further consideration. Carbon steel cable and Kevlar fiber have acceptable hoop height requirements although Kevlar represents almost 70% reduction of hoop height when compared with steel. However, the low energy storage density of carbon steel cable makes it unattractive as a candidate for construction of a flexible rotor.

A hoop constructed of Kevlar-29 capable of storing 50 KWh would weigh about 810 pounds and operate with a maximum rpm of 14,600. The resulting rotor would have a 3' major radius and would be a nominal 8" thick by about 10.4 inches in height. Based on material costs, the 1500-Den Kevlar-29 fiber would be the best choice among the various sizes available.

It has been shown that in order to overcome the subsynchronous whirl instability of the flexible flywheel, the motor/generator must be gimballed on nonintersecting axes to provide the important parameters for whirl stability, namely, low support stiffness, stiffness asymmetry, and bearing support mass (the motor itself). In order to place the motor/generator on the outside of the vacuum vessel, a vacuum feedthrough with three degrees of rotational freedom, two for the gimballing action plus one for rotation of the rotor, would be required. Such a feedthrough would be costly to design and build and could adversely affect the whirl stability parameters. Therefore, as a result of the gimballing requirements, the motor/generator must be placed inside the vacuum vessel. Since a number of motor/generators have been designed within the last

58

TABLE 4. Calculated Values for 50 KWh 6-foot Diameter Flywheel (Fig. 1)

Material	Hoop Weight (lbs.)	Maximum RPM*	Hoop Height (L in ft.)	Storage Energy Density (Wh/lb)	Material Costs $/Wh
Nylon					
1/4"	4718	6058	8.13	10.60	
3/8"	4909	5939	8.22	10.19	
1/2"	4933	5925	8.24	10.14	
Dacron					
1/4"	6487	5167	8.13	7.71	0.265
3/8"	6426	5191	8.63	7.78	0.279
1/2"	6451	5181	8.99	7.75	0.286
High strength carbon-steel cable					
1/4"	10,471	4067	2.59	4.78	0.433
3/8"	10,517	4058	2.60	4.75	0.243
1/2"	10,613	4039	2.64	4.71	0.194
Kevlar 29 Fiber					
200 Den	809.5	14,626	0.860	61.77	0.364
400 Den	811.7	14,607	0.862	61.60	0.248
1000 Den	811.8	13,606	0.862	61.54	0.163
1500 Den	811.8	14,606	0.861	61.59	0.138

* Safety factor = 2

59

decade for high speed operation in a vacuum, this requirement should present no major problem.

Additional requirements placed on the motor/generator are 10 KW peak power output and constant power operation over at least a 2:1 speed range.

If it were not for the requirement of operation in a vacuum, hydrodynamic (fluid film) bearings would be ideal for energy storage flywheel applications. However, the lubricating fluid required would vaporize to some extent and necessitate greater pumpdown requirement. Any seal which might be used to overcome this problem would add unacceptable amounts of power loss thereby reducing the useful energy storage period.

A major disadvantage of ball bearings for flywheel applications is the cage and retainer instabilities which appear at high speeds. Research reported by Eisenhaure and Kingsbury (Reference 4) has shown that this disadvantage can be overcome by using retainerless bearings. Thus, the retainerless precision ball bearing appears to be well suited to the energy storage flywheel system. However, these bearings also require a light film of lubricant for operation.

Magnetic bearings offer the advantage of needing no lubricant and have been shown to have very low drag and long life. Power for the bearing can be supplied by auxiliary windings on the motor generator allowing failsafe spin down operation. Mechanical touchdown bearings would only be needed for cold start/stop situations. Although magnetic bearings are more costly than other alternatives, the cost would more than be offset over the life of the system in decreased maintenance costs.

Elements Subject to Economic Trade-offs

While the need for operating a higher performance energy storage flywheel in a vacuum is not subject to economic trade-offs, the method of providing and maintaining the vacuum is. These trade-offs affect the vacuum vessel, vacuum

system and as mentioned previously, the use of lubricated or oil free bearings.

The vacuum vessel performs a dual role: 1) to provide a low drag environment for the rotor; and 2) to provide a support structure from which to suspend the motor/generator and rotor assembly. In addition, if the system is installed above ground, the vacuum vessel must provide safety containment should a catastrophic failure occur. Two major options exist for the construction vessel, steel or reinforced concrete.

The steel vessel is designed to provide ease in final assembly and installation of the system. The vessel is comprised of two sections. The lower section consists of a steel cylinder having semihemispheric bottom and a ring flange on the top to mate with the upper section which is also semihemispherical. It contains all the necessary feedthroughs and support structures for the motor/generator and rotor assembly. Also provided on the upper section is the pumpdown port. This arrangement allows the entire system to be assembled on the upper section, then lowered into the lower section of the vacuum vessel. The two sections are then welded together at the mating flanges. This design also has the advantage, should the motor/generator or rotor fail, only the upper section need be removed, by cutting the weld, for repair or replacement.

The steel vessel offers the advantage of low outgassing and very low porosity, thus decreasing the vacuum maintenance requirements. When installed below ground the steel cylinder need only be 1/4" thick with the surrounding earth providing failure containment. However, when installed above ground, the thickness must be increased to 5/8" to provide sufficient containment during failure.

The concrete vessel uses the same upper head assembly with its associated advantages. The lower section, however, is constructed of 2" thick reinforced concrete with a thin outer shell of steel. The outer shell provides the mating flange for welding to the upper head. The shell is also needed because of the

high porosity in the concrete, which would allow air to diffuse into the vacuum chamber. This shell need only be about 1/32" thick with the concrete providing all the needed structural strength.

The main advantage of the concrete vessel is realized in above ground installation where the concrete provides the needed failure containment. Unfortunately, concrete outgasses in a vacuum raising pumping requirements to the point where continuous on-site pumping is required.

In order to keep windage drag down to acceptable limits, a vacuum of better than 10 microns (10^{-2} torr) is required. To maintain this vacuum, the pumping system can be either on-site (continuous) or brought to the site as needed periodically. Continuous on-site pumping extracts a price of higher initial capital outlay for the system. In addition, energy must be supplied to the pumping system for operation thereby lowering the overall system efficiency. Therefore, the on-site system should only be used where required as in the concrete vessel option. The on-site vacuum system would consist of a mechanical roughing pump just large enough to overcome the leaks and outgassing at the 10 micron level. Initial pump down would be done at the time of installation by a unit brought to the site for that purpose.

In the periodic pumping scheme, the vacuum system would be brought to the site twice a year. A nationwide network of companies could provide this service as is presently done with many other services nowadays. The service equipment, consisting of a truck containing a diffusion-pump based vacuum system, would be brought to the site and hooked up to the vacuum port. The system would then be pumped down to 10^{-5} torr and valved off. When the pressure reached 10^{-2} torr, the process needs to be repeated.

The advantages of a permanent magnet (PM) DC motor/generator design for high-speed applications are high efficiency and relatively simple power conditioning electronics. The next best candidates are the functionally similar Lundell

62

and Nadyne homopolar inductor designs with the field supplied by a stationary coil, and without brushes or slip rings. However, in addition to field coil power dissipation, the latter designs are heavier and bigger than their PM counterparts and may therefore produce side loading forces which are a problem for magnetic bearing systems. The advantage of a controllable field over a PM field is often offset by the need for more complex and expensive power conditioning electronics. The primary disadvantage of PM units for energy storage devices is the electromagnetic drag due to stator eddy currents.

A brushless-DC PM motor/generator, under development by A. R. Millner of MIT/Lincoln Laboratory (Reference 3), avoids the eddy-current problem by using a truly ironless armature. The only conducting material in the stator is the copper, and this is made of small conductors individually insulated for minimum eddy current losses. Figure 21 shows the layout of the Lincoln Laboratory motor/generator with magnetic bearing. This motor/generator design appears to be a good match for the dual tasks of solar energy storage and conversion. Used in conjunction with the PM motor/generator, a naturally commutated DC input bridge can closely track the maximum power point of the energy source, thereby eliminating mismatches that lower system efficiency. Furthermore, using a cycloconverter, a good quality 60 Hz AC output for the load can be produced.

Even through MIT's motor/generator design has high efficiency (on the order of 90%) it is felt that more cooling will be needed than can be provided by conduction through the frame, gimbal and support structure. This is provided by "canning" the stator armature and flowing transformer oil around the windings.

The oil cooling system consists of a heat exchanger, pump and flexible oil lines to the motor (so as not to inhibit the gimballing action). By assuming 1 KW of heat must be removed (based on 90% efficiency 10 KW input output), a flow rate of .25 gal/min would be sufficient to limit the temperature rise in
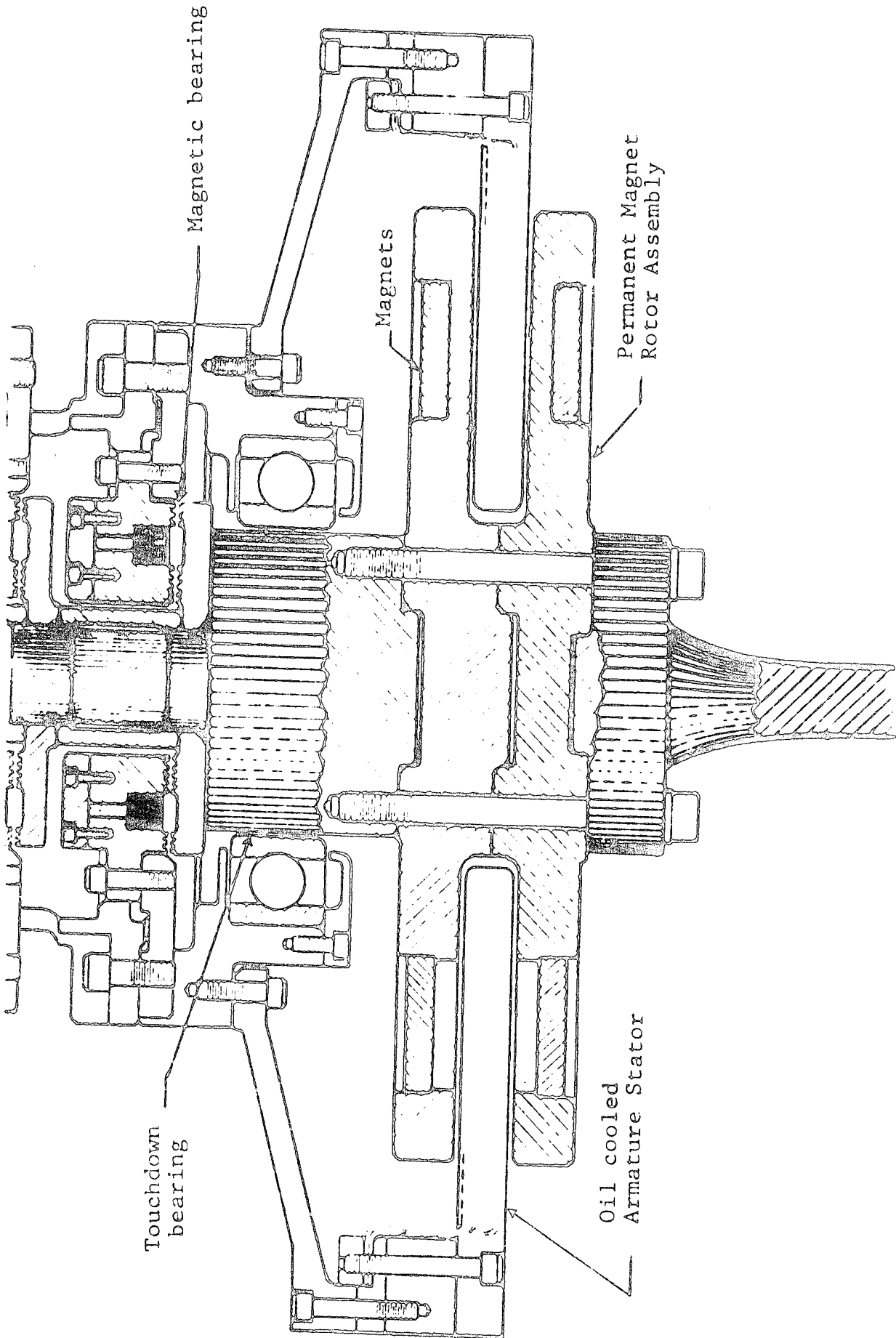
Figure 21. Lincoln Laboratory Motor Generator.

Magnetic bearing

Magnets

Permanent Magnet
Rotor Assembly

Touchdown
bearing

Oil cooled
Armature Stator

the oil to less than 20°C. A small oil pump consuming less than 200 watts would be sufficient to provide the needed flow rate.

The heat exchanger offers two options, air cooled or water cooled. The air cooled option offers the advantage of being a passive heat exchanger, the cooling being provided by natural convection. Unfortunately, this necessitates a much larger surface area to dissipate the heat. The water cooled unit, while smaller in size, requires a ready source of water such as a lake or stream. If the water is available, this option, by far, would be the choice; however, if the water must be supplied by a well, the energy expended by pumping the water would be unacceptable.

The question arises, should the energy storage system provide the output in the form of AC or DC power? The AC option offers the advantage of not having to make any change at the user end of the system. By providing 60 Hz 220V power to residential users, the system could be backfitted easily to present home systems. Also, when backup power from a utility was needed, a simple switch-over could be accomplished. The disadvantage would be the cost of the cyclo-converter needed to convert the output of the flywheel to AC.

On the other hand, DC output could provide most of the energy needs in the average home. All heat producing products, such as stoves, water heaters, furnaces, etc., could run on DC power. Inverters for units requiring AC power such as motors and compressors or electronic devices like T.V. could be provided individually. However, this creates the problems of a dual electrical system, one for DC operating units and the other for the AC units. Also, should backup power be needed from a utility, it would have to be rectified and conditioned to run in the DC electrical units.

Let's now consider two possible systems based on the previous design require-ments. System A would be an above ground installation and System B would be below ground.

System A would consist of a concrete vessel sitting above ground. This would be a major advantage in rocky areas where below ground installation would be prohibitively expensive. As mentioned previously, this system would require an on-site continuous vacuum system. For comparative purposes, this system will utilize the DC electrical output option.

System B is a below ground steel vessel unit. The system utilizes a periodic pumpdown vacuum scheme and AC electrical output. Table 5 gives the comparable system costs of the options for production model quantities of 10,000 units per year.

The motor/generator, magnetic bearings, and associated electronics costs were obtained from Reference 3. These costs, based on 1979 technology, are: 1) the motor/generator, $1000 @ $100/KW; 2) the magnetic bearings, $3750 @ $75/KWh; 3) the electronics, $1600. The costs of the two systems (1979 $) are comparable; System A $24,241 ($485/KWh) and System B, $24,160 ($483/KWh).

To get a better comparison of the two systems, a cost analysis based on the Life-Cycle Cost Methodology of Reference 5 was performed. Input for the analysis is shown in Table 6.

The methodology computes the residential total present value (1985 year of operation selected) and total annual costs including all the parameters listed in Table 6. The cost analysis reveals the following values:

	System A	System B
Total Present Value (1979 $)	$44,642	$36,437
Total Annual Cost	$ 5,244	$ 4,280

The cost difference between the two systems primarily arises from the higher initial and annual costs of a continuous on-site vacuum system.

TABLE 5. Cost Breakdown (1979 Dollars) of System A and B (50 KWh) for
Production-Model Quantities of 10,000 units/year

		System A*	System B*
Rotor		$ 6,885	$ 6,885
Motor/Generator		1,000	1,000
Bearings		3,750	3,750
Gimbal		2,125	2,125
Support Structure		1,400	1,400
Input Electronics		800	800
Output Electronics		50	800
Inverters		774	0
Installation and Assembly		1,500	2,000
Oil Cooler		200	200
Vacuum Vessel		3,580	4,850
Vacuum System		1,500	300**
Backup Power System		650	50
	Total	$24,241	$24,160
One Year Maintenance		1,000***	500**

* Based on a 2,000 sq. ft. home with air conditioner, refrigerator, freezer, and electric furnace.

** Vacuum system costs including vacuum valve and system maintenance.

*** Includes cost of operating vacuum pump.

67

TABLE 6. Input for Cost Analysis by Life-Cycle Cost Methodology[**]

	System A	System B
Discount rate (d)[*]	.10	.10
Percent down payment (D)[*]	.20	.20
Energy escalation rate (e)[*]	.07	.07
Backup energy cost (F)	-	-
General inflation rate (g)[*]	.05	.05
Interest rate (i)[*]	.115	.115
Investment tax credit (I)[*]	0	0
Initial system cost (Ic_p)	$24,241	$24,160
Period of analysis (N)[*]	20 yrs	20 yrs
Accounting lifetime (N_D)[*]	-	
Borrowing period (N_M)[*]	30 yrs	30 yrs
Miscellaneous (maintenance) cost (OM)	$ 1,000	$ 500
Property taxes (P)[*]	0	0
Salvage value (SV)[*]	0	0
Income tax rate (t)[*]	.30	.30
Year of operation (yo)	1985	1985
Price year (yp)	1979	1979

[*] Values from "An Analysis of the Current Economic Feasibility of Solar Water and Space Heating," Office of the Assistant Secretary for Conservation and Solar Applications, DOE/CS-0023. January 1978

[**] A. M. Perino, "A Methodology for Determining the Economic Feasibility of Residential or Commercial Solar Energy Systems," Sandia Laboratories, SAND 78-0931, January 1979.

Summary of Best Option

The conceptual design of a 50 KWh Flexible Flywheel Energy Storage System is shown in Figure 22. The system is designed for below ground installation although above ground or partially below ground installation would represent only minor changes and not greatly affect the cost of the system. The system stores a nominal 50 KWh with a peak output of 10 KW AC.

The major components of the system are: 1) the rotor; 2) the gimbal mounted motor/generator, magnetic bearing and electronics; 3) the oil cooling system; and 4) the vacuum vessel.

The rotor is a simple hoop constructed by coiling Kevlar fibers into a circle 6' in diameter with a minor radius of 4". To maintain shape integrity when not spinning, an outer rope sheath surrounds the cross-section of the hoop. The overall hoop assembly weighs 850 pounds and stores a nominal 50 KWh at 14,000 rpm. Maximum rpm is 14,600 with a safety factor of 2. Four flexible ropes attach the hoop to the motor/generator shaft.

The oil cooling system consists of a radiator, oil pump and flexible lines to the motor/generator. The radiator is an oil-to-air cooling unit similar to those found in large cars and trucks. A small oil pump is included to provide flow in the systems. Because the pressures involved would be low, the pump would only have to overcome small head losses and only require 50 to 100 watts of power. The flexible lines are needed to allow free movement of the motor generator in its gimbal mounts. The system uses insulating transformer oil to eliminate the possibility of shorting out the armature stator.

The vacuum vessel is designed to provide ease in final assembly and installation of the system. The vessel is comprised of two sections. The lower section consists of a 1/4" thick steel cylinder with a semihemispherical bottom. The upper section, also semihemispheric, contains all necessary feedthroughs for
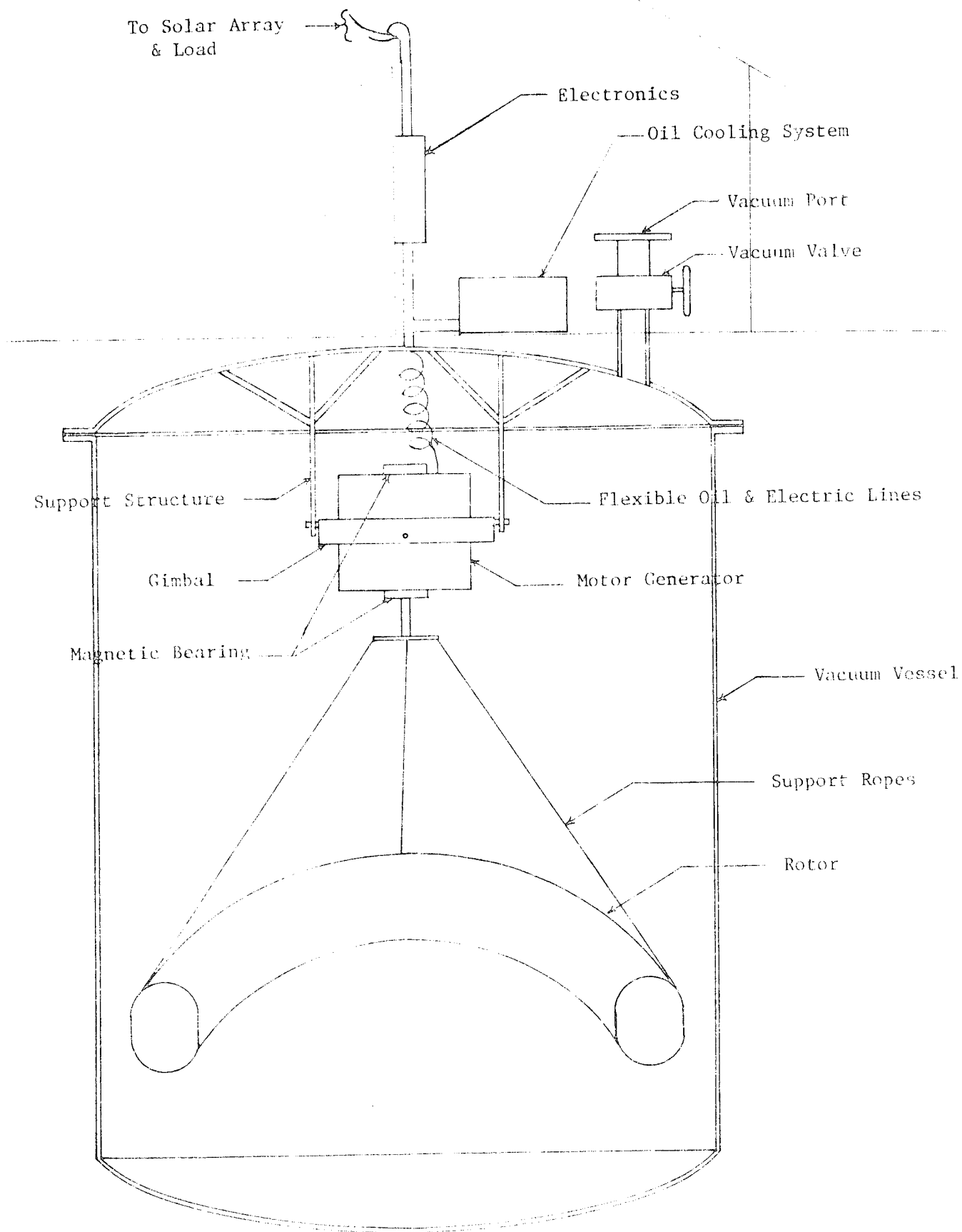
Figure 22. Conceptual Design of a 50 KWh Flexible Flywheel Energy Storage System.

the electric oil lines and the support structure for the motor generator and rotor assembly. Also provided is a pumpdown port and vacuum valve. This arrangement allows the entire system to be assembled on the upper head then lowered into the rest of the vacuum vessel. The two sections are then welded together at the mating flanges either at the manufacturing plant or at the installation site. This design also has the advantage, should the motor-generator or rotor fail, that only the upper section need be removed, by cutting the weld, for unit repair or replacement instead of removing the entire vacuum vessel from its below ground installation.

A motor/generator similar to the one being developed at MIT/Lincoln Laboratory (A. R. Millner) will be used. A significant departure from Millner's design is to "can" the stator armature to enable cooling of the windings with transformer oil. The MIT motor/generator is being developed under the sponsorship of the U. S. Department of Energy (DOE), specifically for flywheel applications interfaced with solar photovoltaic systems.

The selected motor/generator is of a brushless-DC, permanent magnet design offering the advantages of high-efficiency and relatively simple power conditioning electronics for high speed applications. Oil cooling of the stator armature was added to the design because it is believed that conduction through the frame and gimbal support structure would provide insufficient cooling. Futher detail on the motor/generator as well as the bearings and electronics can be found in Reference 3.

The magnetic bearings were chosen over ball bearings to avoid the necessity of bearing lubrication. In the case of ball bearings, the oil film would constantly be boiling off into the vacuum chambers, necessitating constant oil replacement and more frequent vacuum vessel pumpdown, both resulting in higher maintenance costs. These maintenance cost increases would more than offset,

71

over the life of the system, the higher cost of the magnetic bearings (based on the life-cycle costing methodology used in the cost analysis). The bearings can be powered by auxilliary windings on the motor, allowing fail-safe spin-down operation. Mechanical touchdown bearings are included for cold start/stop situations.

The electronics interface between the DC solar array and the PM motor/generator provides high quality 60 Hz AC for residential power consumption. All solar/electric power would go into the motor/generator to spin up the rotor. The motor/generator would be electronically controlled to serve as a maximum power tracker. This is important because the varying electrical output of solar arrays is generally mismatched to the characteristics of the storage system and load, causing inefficient operation. The generator output is fed into a silicon controlled rectifier (SCR) cycloconverter which, with a transformer, provides 220V/60 Hz output to the load.

Table 7 gives a comparative cost breakdown, in 1979 dollars, of a 10 KWh prototype flywheel system and the 50 KWh system B production model of Table 6. Major cost items are: 1) the rotor; 2) the motor/generator; 3) the magnetic bearings; 4) the electronics and 5) the vacuum vessel. The rotor is constructed of 1500-Den Kevlar at a cost of $8.00 per pound. This results in a cost of $6800 (850 lbs.) for the 50 KWh (production model) rotor and $1296 (162 lbs.) for the 10 KWh prototype. Rotor construction costs are estimated to be $0.10 per pound or $85 for the production model and $1.00 per pound or $162 for the prototype. The total rotor costs are then $6885 for the 50 KWh rotor and $1458 for the 10 KWh prototype rotor. It should be noted that a large savings can be realized if the cost of Kevlar decreases in the future ($850 for each dollar reduction in the price per pound.)

TABLE 7. Cost Breakdown (1979 Dollars) for Prototype and Production Model

	10 KWh (Prototype)	50 KWh (Production Model) (10,000 unit/year)
Rotor	$ 1,458	$ 6,885
Motor/Generator	1,000**	1,000*
Electronics	1,600**	1,600*
Bearings	1,250**	3,750*
Vacuum Vessel	5,150	5,150
Gimbal	850	2,125
Support Structure	500	1,400
Installation & Assembly	1,000	2,000
Oil Cooler	100	200
Backup Power Switchover	-	50
	$12,680	$24,160

Prototype Engineering
Services $1,500.00

Testing $1,500.00

Maintenance $500/yr
based on 2 pumpdowns
per year

* A. R. Millner, "A Flywheel Energy Storage and Conversion System for Solar
       Photovoltaic Applications," ASME, 79-501-1, March 1979.

** Prices higher per KWh due to one of a kind prototype.

The costs per KWh for the 50 KWh production model are significantly lower than for the 10 KWh prototype due to the dual benefits of scale and quantity production--$20 vs. $100 for the motor/generator, $75 vs. $125 for the bearings and $32 vs. $160 for the electronics. Again, these areas are subject to cost reductions with advances in technological development.

The cost of the vacuum vessel are determined based on 1979 costs of steel vessels of similar dimensions. This cost is $5,150 and quite subject to fluctuations in the price of steel.

CONCLUSIONS

The principal conclusions from this research can be summarized as follows:

(1) Subsynchronous whirl instability at supercritical speeds due to internal friction is strongly suppressed by a gimballed motor/ generator support system. (This finding is applicable to more conventional flywheels as well.)

(2) A flexible flywheel made from synthetic rope or fiber with no bonding agent is easy to construct and can be made self-balancing by a properly designed support system.

(3) The flexible flywheel system offers a relatively inexpensive and efficient tool for investigating flywheel rotor dynamics in general, since:

(a) failures are not catastrophic

(b) critical speeds are so low that whirl modes can be visually observed, and

(c) support rope configurations can be varied to approximate the shaft constraints of conventional flywheels.

(4) The simplicity of the flexible flywheel construction promotes economical production using conventional manufacturing processes and equipment.

REFERENCES

1. Smith, B. T., Boyle, J. M., Garbow, B. S., Ikebe, Y., Kleme, V. C. and Moler, C. B., Matrix Eigensystem Routines, Springer-Verlag, 1974.

2. Wilkinson, J. H., The Algebraic Eigenvalue Problem, Clarendon Press, Oxford, 1965.

3. Millner, A. R., "A Flywheel Energy Storage and Conversion System for Solar Photovoltaic Application," ASME paper 79-Sol-1 Gas Turbine and Solar Energy Conference, San Diego, California, March 12-15, 1979.

4. Eisenhaure, D. B., and Kingsbury, E. P., Final Report on the Development of an Advanced Flywheel Bearing Performance Model, Sandia Laboratories, SAND 79-7003, March, 1979.

5. Perino, A. M., A Methodology for Determining the Economic Feasibility of Residential or Commercial Solar Energy Systems, Sandia Laboratories Report SAND 78-0931, January, 1979.

6. Lanczos, C., The Variational Principles of Mechanics, University of Toronto Press, Toronto, 1966.

APPENDIX A

Flexible Flywheel Sizing and Performance Calculation

1. On the Breaking Speed and Maximum Storable Energy in a Stranded Hoop Flywheel

The maximum energy E which can be stored in a stranded hoop flywheel without breaking it is a function only of the mean hoop radius R and the total tensile proof load P of the hoop fibers (cumulative strength).

The maximum speed N_E corresponding to E, however, is also a function of the lineal weight per unit length w of the hoop material.

The design equation for maximum storage energy is:

$$E = \pi RP \ \text{ft-lb.}$$

or

$$E = \frac{\pi RP}{(2.654)(10^6)} \ \text{KWh}$$

where R = ft.

P = lb.

The maximum speed is given by

$$N_E = \frac{60}{2\pi} \sqrt{\frac{Pg}{\overline{w}R^2}}$$

where g = 32.2 ft/sec^2

$\overline{w}$ = lb/ft.

It can be seen that, although the material weight $\overline{w}$ does not affect the maximum energy E, a practical advantage of a heavy material is that it develops its maximum energy at a lower speed, thus reducing windage and friction losses. Also, currently available electrical machinery is speed limited.

The dimensions of a flywheel for home energy storage are limited by space available for the unit. A practical maximum radius (R) seems to be about 3 feet. If the hoop cross section radius is more than about 4 inches, the flywheel is no longer a "hoop", the equations above do not apply, and the safety advantages of individual independent strands are probably lost by some required bonding or tying of the fibers. Thus the cross sectional area of a hoop with circular cross section is limited to about 16 πin^2.

For a flywheel of 3 feet radius and given material, the only available way to increase the cumulative proof load P (and E) is to increase the axial length L of the hoop (thus making the flywheel a long hollow cylinder). The practical limit on L is probably about 4 feet. A long L, however, introduces another dynamic whirl mode into the system, with its potential instability. Therefore L should be kept as short as possible.

2. Calculation of Size and Performance in Terms of Hoop Radius R

In sizing a flexible flywheel, it is helpful to have performance and design parameters expressed in terms of the hoop radius R.

The following calculations give the maximum energy stored $\overline{E}$, corresponding speed N_E, hoop weight W, energy density, cost, cost/KWh, and bearing power loss in terms of the hoop radius R. Also given are the absolute values for a 2 ft. radius hoop, as an example for comparison of the effect of material.

The calculations are made for DACRON^R 1/4" rope, KEVLAR^R 1/4" rope (hand construction), and KEVLAR^R - 49-1429 Denier fiber (machine construction). All calculations contain a factor of safety - 2.0.

A. DACRON^R Wheel (1/4" ϕ rope), F.S. = 2

For 8" ϕ cross section ($\overline{W}$ = .022 lb/ft):

$$A = \frac{\pi 8^2}{4} = 50.26 \text{ in}^2$$

$$P_{strand} = 1800 \text{ lb.}$$

$$N_{strands} = \frac{50.26}{.049} \times .8 \left(\begin{array}{c}\text{density}\\\text{factor}\end{array}\right) = \underline{820} \text{ strands, where .049 is c/s area per strand}$$

$$P = (820)(1800) = 1.476 \times 10^6 \text{ lb.}$$

$$\overline{E} = \frac{R\pi \frac{P}{2}}{(2.654)(10^6)} = (.8735)R \text{ KWh, where P/2 reflects a factor of safety of 2}$$

$$N_E = \frac{60}{2\pi R} \sqrt{\frac{\frac{P}{2}(g)}{\overline{W}}} = \frac{60}{2\pi R} \sqrt{\frac{(.738)(10^6)(32.2)}{(.022)(820)}} = 10,960/R \text{ rpm}$$

$$W = 2\pi R N_{strands} \quad \overline{W} = (2\pi)(820)(.021 \text{ lb/ft}) \ R = 113 \ R \text{ lb}$$

$$\ell = 2\pi R N_{strands} = (2\pi)(820)R = 5152R \text{ ft.}$$

$$\text{Energy Density} = \frac{873.5R}{113R} \frac{\text{KWh}}{\text{lb.}} = 7.73 \frac{\text{watt-hr}}{\text{lb.}}$$

Cost = .18\$/ft. x 5152R ft. = \$927R

$$\frac{\text{Cost}}{\text{KWh}} = \frac{927\text{R}}{.8735\text{R}} \frac{\$}{\text{KWh}} = \frac{\$1062}{\text{KWh}}$$

Bearing Power Loss (1-1/4" shaft, Fig. 9, Ref. 4)

$$E_L = .035 \frac{\text{watts}}{\text{lb-1000 rpm}}$$

or

$$\overline{E}_L = .035 \frac{\text{watts}}{\text{lb-1000rpm}} \text{ x } \frac{1}{.00773} \frac{\text{lb}}{\text{KWh}} = 4.53 \frac{\text{watts}}{\text{KWh-1000rpm}}$$

For R = 2'

Store 1.747 KWh @ 5480 rpm

Weight = 226 lb.; 10,304 ft of 1/4" rope

Flywheel Cost = \$1855, Bearing Power Loss = 45 watts

B. KEVLAR^R Wheel (1/4" ϕPhillystran Rope)

For 8" cross section ($\overline{W}$ = .021 lb/ft):

$$A = \frac{\pi 8^2}{4} = 50.26 \text{ in}^2$$

$$P_{strand} = 6750 \text{ lb.}$$

$$\sigma = 6750\text{lb}/.049 \text{ in}^2 = 137,755 \text{ psi}$$

$$N_{strands} = \frac{(50.26)(.8)}{.049} \text{ (density factor)} = \underline{820} \text{ strands}$$

$$P = (820)(6750) = 5.53 \times 10^6 \text{ lb.}$$

$$\overline{E} = \frac{R\pi \frac{P}{2}}{(2.654)(10^6)} = (3.28)\text{R KWh}$$

$$N_E = \frac{60}{2\pi R} \sqrt{\frac{\frac{P}{2}(g)}{\overline{W}}} = \frac{60}{2\pi R} \sqrt{\frac{(2.768 \times 10^6)(32.2)}{(.021)(820)}} = 21,735/\text{R rpm}$$

$$W = 2\pi R N_{strands} \quad \overline{W} = (2\pi)(820)(.021 \text{ lb/ft})R = (108)R \text{ lb}.$$

$$\ell = 2\pi R N_{strands} = (2\pi)(820)R = (5152)R \text{ ft}.$$

$$\text{Energy Density} = \frac{3280R}{108R} \frac{(\text{watt-h})}{(1b)} = 30.37 \frac{\text{watt-h}}{1b}$$

$$\text{Cost} = \frac{.60\$}{\text{ft}.} \times 5152R \text{ ft}. = 3091R\$$$

$$\frac{\text{Cost}}{\text{KWh}} = \frac{3091R}{3.28R} = \frac{\$942}{\text{KWh}} \text{ (hoop only)}$$

Bearing Power Loss (1-1/4" shaft, Fig. 9, Ref. 4)

$$E_L = .035 \frac{\text{watts}}{1b\text{-}1000 \text{ rpm}}$$

$$\overline{E}_L = 0.35 \frac{\text{watts}}{1b\text{-}1000\text{rpm}} \times \frac{1}{.03037} \frac{1b}{\text{KWh}} = 1.152 \frac{\text{watts}}{\text{KWh-}1000\text{rpm}}$$

For R = 2'

Stores 6-1/2 KWh @ 10,862 rpm

Weight = 216 lb.; 10,304 ft of 1/4" rope

Flywheel Cost = $6182, Bearing Power Loss = 82 watts

C. KEVLAR[R] Wheel (1420 Den. Kevlar-49) F.S. = 2

For 8" cross section (density (λ) is .052 lb/in^3):

$$A = \frac{\pi 8^2}{4} = 50.26 \text{ in}^2$$

$$P_{strand} = 68.81 \text{ lb}$$

$$\sigma = \frac{68.81 \text{ lb}.}{1.68 \times 10^{-4} \text{ in}^2} = 409,600 \text{ psi}$$

$$N_{strands} = \frac{(50.26)(.9)}{(.000168)} = 269,290 \text{ strands}$$

$$P = (269,290)(68.81) = 18.53 \times 10^6 \text{ lb}$$

$$\overline{E} = \frac{R\pi \frac{P}{2}}{(2.654)(10^6)} = (10.97)R \text{ KWh}$$

$$N_E = \frac{60}{2\pi R} \sqrt{\frac{(\frac{P}{2})g}{\overline{w}}} = \frac{60}{2\pi R} \sqrt{\frac{(18.53)(10^6)(32.2)}{(2)(28.3)}} = 31,005/R \text{ rpm}$$

$$\overline{w} = (\lambda)(A)(12)(.9) = 28.29 \text{ lb/ft}$$

$$W = (\lambda)(A)(2\pi R)(12)(.9) = 177.35R \text{ 1b}$$

$$\text{Energy Density} = \frac{10,970R \text{ watt-h}}{177.35R \text{ 1b.}} = 61.85 \frac{\text{watt-h}}{16}$$

$$\text{Cost} = \$8.50/1\text{b. x } 177.35R \text{ 1b.} = 1507R\$$$

$$\frac{\text{Cost}}{\text{KWh}} = \frac{1507R}{10.97R} = \$137/\text{KWh}$$

Bearing Power Loss (1-1/4" shaft, Fig. 9, Ref. 4)

$$E_L = .035 \frac{\text{watts}}{\text{1b-1000rpm}} \text{ x } \frac{1}{.061} \frac{\text{1b}}{\text{KWh}} = .574 \frac{\text{watts}}{\text{KWh-1000rpm}}$$

$$\overline{E}_L = .035 \frac{\text{watts}}{\text{1b-1000rpm}} \text{ x } \frac{1}{.061} \frac{\text{1b}}{\text{KWh}} = .574 \frac{\text{watts}}{\text{KWh-1000rpm}}$$

For R = 2'

Stores 22 KWh @ 15,500 rpm

Weight 355 1b.

Cost = $3015 (Material only)

Bearing Power Loss = 196 watts

APPENDIX B FLYWHEEL EQUATIONS OF MOTION

The flywheel's differential equations of motion are best derived by way of Lagrangian mechanics. The general form of Lagrange's equation of motion is

$$\frac{d}{dt}\left(\frac{\partial L}{\partial \dot{q}_i}\right) - \frac{\partial L}{\partial q_i} = Q_i \qquad \text{for } i = 1, 2, \ldots, n$$

where the Lagrangian, L, is the difference between the kinetic energy of the system, T, and the potential energy of the system, V.

$$L = T - V$$

The Q_i is the generalized nonconservative force acting on the ith coordinate, q_i, and n is the number of degrees of freedom.

An exact expression for the system's total kinetic energy while in a completely arbitrary configuration described by the five generalized coordinates shown in Figure B1 is

$$T = \tfrac{1}{2}M_1 v_{G_1}^2 + \tfrac{1}{2}M_2 v_{G_2}^2 + \tfrac{1}{2}I_B \dot{\alpha}^2 + \tfrac{1}{2}(\bar{I}_C + \bar{I}_A)(\dot{\beta}^2 + \dot{\alpha}^2 \cos^2\beta) + \tfrac{1}{2}(I_C + I_A)\dot{\alpha}^2 \sin^2\beta$$

$$+ \tfrac{1}{2}I_A \omega^2 + I_A \omega \dot{\alpha} \sin\beta + \tfrac{1}{2}I_X(\dot{\phi}^2 \sin^2\phi + \dot{\phi}^2) + \tfrac{1}{2}I_Z(\dot{\phi}\cos\phi + \dot{\psi})^2$$

where v_{G_1} is the translational velocity of the motor mass center, G_1,

$$v_{G_1}^2 = (h + \overline{OG}_1 \cos\beta)^2 \dot{\alpha}^2 + (\overline{OG}_1 \dot{\beta})^2$$

and v_{G_2} is the translational velocity of the flywheel mass center, G_2,

$$v_{G_2}^2 = (h + \overline{OS}\cos\beta)^2 \dot{\alpha}^2 + \overline{OS}^2 \dot{\beta}^2 + \ell^2 \sin^2\theta \dot{\phi}^2 + \ell^2 \dot{\theta}^2 + 2\ell(h + \overline{OS}\cos\beta)\dot{\alpha}$$

$$(\dot{\theta}\cos\theta\sin(\phi-\alpha) + \dot{\phi}\sin\theta\cos(\phi-\alpha)) + 2\ell\,\overline{OS}\,\dot{\beta}\sin\beta\,(\dot{\phi}\sin\theta\,\sin(\phi-\alpha)$$

$$- \dot{\theta}\cos\theta\cos(\phi-\alpha)) + 2\ell\overline{OS}\dot{\theta}\dot{\beta}\sin\theta\cos\beta$$

These two terms in T express the overall system translational kinetic energy. The remaining terms in T are the various components of the system rotational kinetic energy.

An exact expression for the system's total potential energy is

$$V = -M_B g b \cos\alpha - (M_1 + M_2) gh\cos\alpha - (M_1 \overline{OG}_1 + M_2 \overline{OG}_2) g \cos\beta \cos\alpha$$

$$- M_2 g \ell \cos\phi \sin\theta + \tfrac{1}{2} k_\alpha \alpha^2 + \tfrac{1}{2} k_\beta \beta^2$$

The various length parameters appearing in these expressions are defined in Figure B1, except for b which is the distance from point Q to the center of mass of the horseshoe shaped gimbal bracket. The various properties are defined as follows:

M_1 - mass of the motor, including any shaft and any motor hub to which the support ropes may be fastened

M_2 - mass of the flywheel

M_B - mass of gimbal bracket

I_B - rotational inertia of gimbal bracket about point Q

I_C - rotational inertia of the motor's non-rotating parts, mainly the housing, taken about the motor's main, longitudinal axis

$\overline{I}_C$ - rotational inertia of motor's non-rotating parts about a transverse line passing through the motor mass center, G_2

I_A - rotational inertia of motor's rotating parts, mainly the armature, shaft and hub, about main longitudinal axis

$\overline{I}_A$ - rotational inertia of motor's rotating parts about a transverse line passing through G_2

I_Z - rotational inertia of flywheel about its main axis of rotation

I_X - rotational inertia of flywheel about a transverse line

g - acceleration due to gravity

With the above expression for the Lagrangian the left-hand side of Lagrange's equation of motion can now be obtained. The generalized nonconservative forces appearing on the right-hand side are obtained from an expression for the virtual work done by all the nonconservative forces present in the system as the system is displaced through a virtual displacement. For the flywheel system the nonconservative forces are air drag acting on the flywheel, internal hysteresis in the support ropes and frictional damping on the two gimbal axes of rotation. For a more thorough treatment of the Lagrangian method of analytical mechanics see Reference 6.

A. Rigid Shaft Model

By taking the derivatives indicated by Lagrange's equation, along with the nonconservative forces, one obtains a set of extremely long and highly non-linear differential equations. The solution to these equations, if it could be obtained, would be an exact expression for every possible motion the system can have under the action of the assumed nonconservative forces. For the purpose of using the flywheel as an energy storage device one does not need to know all the possible motions. It will be sufficient to know whether or not pure spin about the vertical axis is a dynamic equilibrium for the system, and if so, whether or not this equilibrium is stable. This is done by approximating all the non-linear terms to be linear for small magnitudes of motion about the equilibrium configuration in question. This will reduce the set of non-linear differential equations to a set of linear differential equations which can be solved by applying linear oscillation theory.

For the rigid shaft model this set of linearized differential equations for the case of constant motor speed, ω, is

$$I_Q \ddot{\alpha} + M_2 \ell \ (h + \overline{OS}) \ddot{\phi} + I_A \omega \dot{\beta} + K_\alpha \alpha = (h + \overline{OS})(F_\alpha^G + F_\alpha^S) - C_\alpha \dot{\alpha}$$

$$I_0 \ddot{\beta} + M_2 \ \overline{OS} \ddot{\theta} - I_A \omega \dot{\alpha} + K_\beta \beta = -\overline{OS} \ (F^G + F^S) - C$$

$$I_f^S \ddot{\phi} + M_2 \ell \ (h + \overline{OS}) \ddot{\alpha} + I_z \omega \dot{\theta} + K_\phi \phi = \ell F_\phi^G$$

$$I_f^S \ddot{\theta} + M_2 \ \overline{OS} \ddot{\beta} - I_z \omega \dot{\theta} + K_\theta \theta = -\ell F_\theta^G$$

Each term in these equations represents a torque that is present in the system such as inertia torques, gyroscopic torques, gravity torques and non-conservative torques due to friction. The constants appearing are length parameters shown in Figure B1 and system inertias and springs defined as follows:

$I_Q = I_m^Q + I_f^Q$, effective system rotational inertia about upper gimbal axis through point Q

$I_m^Q = M_1 (h + \overline{OG_1})^2 + \overline{I}_C + \overline{I}_A + I_B$, rotational inertia of motor and support system about upper gimbal axis through point Q

$I_f^Q = M_2 (h + \overline{OS})^2$, effective rotational inertia of flywheel about upper gimbal axis

$I_0 = I_m^0 + I_f^0$, effective system rotational inertia about lower gimbal axis through point O.

$I_m^0 = M_1 \overline{OG_1}^2 + \overline{I}_C + \overline{I}_A$, rotational inertia of motor and support system about lower gimbal axis.
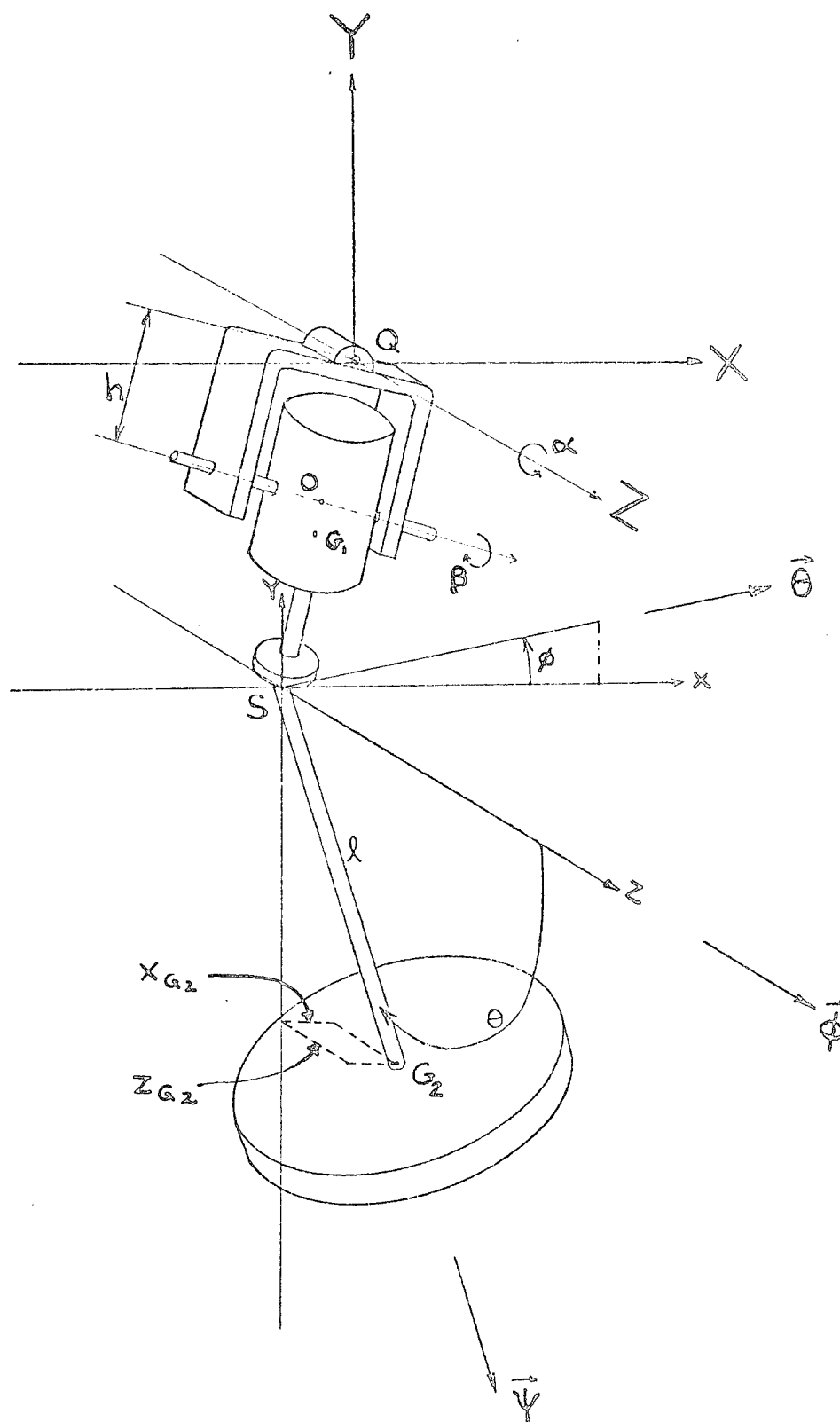
85

Fig. B1. Flexible Flywheel Model With "Rigid-Shaft" Support Ropes
and Gimballed Motor/Generator

$I_f^O = M_2 \overline{OS}^L$, effective rotational inertia of flywheel about lower gimbal axis

$I_f^S = M_2 \ell^2 + I_\chi$, rotational inertia of flywheel about a horizontal line through point S

$K_\alpha = (M_B b + M_1 h + M_2 h + M_1 \overline{OG}_1 + M_2 \overline{OS}) g + k_\alpha$, total spring rate associated with the α coordinate

k_α , spring rate of any spring that is installed in addition to gravity on the α coordinate

$K_\beta = (M_1 \overline{OG}_1 + M_2 \overline{OS}) g + k_\beta$, total spring rate associated with the β coordinate

k_β , spring rate of any spring installed in addition to gravity on the β coordinate

$K_\phi = M_2 \ell g$, gravity spring rate on ϕ coordinate

$K_\theta = M_2 \ell g$, gravity spring rate on θ coordinate

The components of the nonconservative forces are defined as follows:

C_α , viscous damping constant for motion in the α coordinate (torque per angular velocity)

C_β , viscous damping constant for motion in the β coordinate (torque per angular velocity)

$F_\alpha^S = {}^i F_\alpha^S = -C_i [\omega(-\ell\overline{\theta} + \ell\beta) - (\ell\dot{\phi} - \ell\dot{\alpha})]$, internal friction force acting at the motor hub, point S, in the α coordinate

C_i , internal friction constant of proportionality (force per linear velocity)

$\overline{\theta} = \theta - \dfrac{\pi}{2}$

$F_\beta^S = {}^i F_\beta^S = -C_i [-\omega(\ell\phi - \ell\alpha) - (-\ell\dot{\theta} + \ell\beta)]$, internal friction force acting at the motor hub, point S, in the β coordinate

$F_\phi^G = {}^i F_\phi^G + {}^a F_\phi^G$, total nonconservative force acting at flywheel center, G_w in ϕ coordinate

${}^i F_\theta^G = -C i \omega \ell (\phi - \alpha) + C_i \ell(\dot{\theta} - \dot{\beta})$, internal friction force at flywheel center in θ coordinate

${}^a F_\theta^G = C_a (\ell\dot{\theta} + \overline{OS}\dot{\beta})$, air drag force at flywheel center in θ coordinate

87

The difference between the bowed-out rope model and the rigid-shaft model is the configuration of the support ropes. This difference causes two basic changes in the differential equations listed above. First the flywheel will now behave as if it were a point mass. Second, the different geometry of the support ropes changes the action of the internal friction force. These changes are summarized as follows:

$$I_X = 0$$

$$I_Z = 0$$

$$^i F^S_\alpha = -C_i \omega \ell (-\bar{\theta} - f\beta) + C_i \ell (\dot{\phi} - f\dot{\alpha})$$

$$^i F^S_\beta = C_i \omega \ell (\phi + f\alpha) - C_i \omega (\dot{\theta} + f\dot{\beta})$$

$$^i F^G_\alpha = C_i \omega \ell (-\bar{\theta} - f\alpha) - C_i (\dot{\phi} - f\dot{\alpha})$$

$$^i F^G_\beta = -C_i \omega \ell (\phi + f\alpha) + C_i (\dot{\theta} + f\dot{\beta})$$

where the constant f is defined as

$$f = a/(D - a)$$

with

a = diameter of the motor hub where the support ropes are attached

D = diameter of the flywheel where the support ropes are attached

With these changes noted the four differential equations of motion for the bowed-out model are identical to those derived for the rigid-shaft model.

APPENDIX C

Computer Program for Stability Analysis

The eigenvalues and eigenvectors for the matrix A of equation (1) are found by using an International Mathematical and Statistical Library (IMSL) program by the name EIGRF. The program is designed to find the complex eigenvalues and (optionally) eigenvectors of a real general matrix in full storage mode. The algorithm used by this program, see References (1,2) makes use of a number of other IMSL subroutines. The matrix is first balanced to reduce numerical error and then a Hessenberg matrix is found for this balanced matrix. The eigenvalues and eigenvectors are found for the Hessenberg matrix and are then back-transformed into the eigenvalues and eigenvectors for the original matrix A.

Once the eigenvalues, λ, and the eigenvectors, u, have been found, the stability of the system can be deduced directly from the eigenvalues. However, to find the mode shapes from the complex eigenvectors requires some manipulation. First, it should be noted that since matrix A contains only real numbers it can be shown that the eigenvalues will always appear in complex conjugate pairs, and from this it can be shown that the corresponding eigenvectors will also be complex conjugates. Knowing this, the general solution for the state vector, X, can be written as

$$X = B_1 u_1 e^{\lambda \tau} + B_2 \bar{u}_1 e^{\bar{\lambda}_1 \tau} + \ldots + B_{2n-1} u_n e^{\lambda_n \tau} + B_{2n} \bar{u}_n e^{\bar{\lambda}_n \tau}$$

where the B's are complex constants and the bar denotes complex conjugate.

One complex conjugate pair of eigenvalues contributes two independent parts to the general solution, which is also complex. But in the case of the flywheel, which is a real system, the solution needs to be real so that we don't want the entire general solution. For the solution to be real, the constants associated with a conjugate pair of eigenvalues, say B_1 and B_2, must then also be complex conjugates. This will make these two terms of the general solution complex conjugates of each other and therefore yield a real expression upon addition.

There are still two arbitrary constants associated with the pair of eigenvalues, the real part and the imaginary part. To find the mode shape associated with a pair of conjugate eigenvalues, set the real part of the constant equal to one and the imaginary part equal to zero. This will give real numbers for the coordinates of the system, and if desired can be plotted to show the relative whirl orbits of the flywheel and the motor which in general will be elliptical.

A listing of the calling program follows:

TIONS: NODECK,NOLIST,OPT(0),NODUMP

FFECT: NAME(MAIN) NOOPTIMIZE LINECOUNT(60) SIZE(MAX) AUTODBL(NONE)
       SOURCE EBCDIC NOLIST NODECK OBJECT NOMAP NEFORMAT GOSTMT NOXREF ALC NOANSF

```
          COMPLEX*16 LAMBDA(8),Z(8,8),ZN
          DOUBLE PRECISION E(8,8),M1,M2,MB,IB,IA,ICA,IX,IZ,L,H,IMG,IFG,IG,IM
         #O,IFO,IO,IFS,KA,KB,KPHI,KTHE,HOG,HOS,BR,OG,OS,GRAV,CA,CB,CI,CD,CID
         #,W,A,AP,APP,B,BP,BPP,C,CP,CPP,D,DP,DPP,WK(160),F
          DATA E/64*0.0D0/
          READ(5,300)MB,M1,M2,IB,IA,ICA,I,IZ,H,FR,OG,OS,L,GRAV,CA,CB,CI,CD,
         #W
  300     FORMAT(3F10.5,/,5F10.5,/,6F10.5,/,4F10.5,/,F10.5)
          DO 13 II=1,27
          CI=0.0F4D0+0.01D0*(FLOAT(II)-1.0)
  34      WRITE(6,300)MB,M1,M2,IB,IA,ICA,IX,IZ,H,FR,OG,OS,L,GRAV,CA,CB,CI,CD
         #,W
          WRITE(6,350)
  350     FORMAT(1H ,/////)
          HOG=H*OG
          HOS=H*OS
          IMG=M1*(HOG*HOG)+ICA+IB
          IFG=M2*(HOS*HOS)
          IG=IMG+IFG
          IMO=M1*(OG*OG)+ICA
          IFO=M2*(OS*OS)
          IO=IMO+IFO
          IFS=M2*L*L+I
          KA=(MB*BB+M1*H+M2*H+M1*OG+M2*OS)*GRAV
          KB=(M1*OG+M2*OS)*GRAV
          KPHI=M2*GRAV*L
          KTHE=KPHI
          A=-(IFS*IMG+IX*M2*HOS*HOS)/(M2*L*HOS)
          AP=IFS/(M2*L*HOS)
          B=-(IFS*IMO+IX*M2*OS*OS)/(M2*L*OS)
          BP=IFS/(M2*L*OS)
          C=A
          CP=IG/(M2*L*HOS)
          D=B
          DP=IO/(M2*L*OS)
          F=1.875D0/(9.0D0-1.875D0)
          E(1,1)=(AP*CD*HOS*HOS-CD*L*HOS-CI*L*L*F*AP*CA)/A
          E(1,2)=-AP*IA*W/A
          E(1,3)=(AP*HOS*L*CD-(CI*CD)*L*L)/A
          E(1,4)=0.0D0
          E(1,5)=AP*KA/A
          E(1,6)=-CI*W*L*L*F/A
          F(1,7)=-KPHI/A
          E(1,8)=-CI*W*L*L/A
          E(2,1)=-BP*IA*W/B
          E(2,2)=(BP*CD*CS*OS-CD*L*OS-CI*L*L*F*BP*CB)/B
          E(2,3)=0.0D0
          E(2,4)=(-(CI*CD)*L*L*BP*OS*L*CD)/B
          E(2,5)=CI*W*L*L*F/B
          E(2,6)=BP*KB/B
          E(2,7)=CI*W*L*L/B
          E(2,8)=-KTHE/B
          E(3,1)=(-CD*HOS*HOS*CP*CI*L*L*F*CP*CD*L*HOS-CA)/C
```

```
        E(3,2)=-IA*W/C
        E(3,3)=(-CD*L*FOS+CP*L*L*((I+CD))/C
        E(3,4)=0.0D0
        E(3,5)=-KA/C
        E(3,6)=CP*CI*W*L*L*F/C
        E(3,7)=CP*KPHI/C
        E(3,8)=CP*CI*W*L*L/C
        E(4,1)=IA*W/D
        E(4,2)=(-CD*OS*OS+DP*CI*L*L*F+DP*CD*L*OS-CB)/D
        E(4,3)=0.0D0
        E(4,4)=(DP*(CI+CD)*L*L-CD*L*OS)/D
        E(4,5)=-DP*CI*W*L*L*F/D
        E(4,6)=-KB/D
        E(4,7)=-DP*CI*W*L*L/D
        E(4,8)=DP*KTHE/D
        E(5,1)=1.0D0
        E(6,2)=1.0D0
        E(7,3)=1.0D0
        E(8,4)=1.0D0
C=============================================================
        N=8
        IJOB=2
        CALL EIGRF(E,N,N,IJOB,LAMBDA,Z,N,WK,IER)
        DO 5 J=1,N
        ZN=Z(7,J)
        DO 5 I=1,N
        Z(I,J)=Z(I,J)/ZN
5       CONTINUE
        DO 6 I=1,N
        WRITE(6,100)LAMBDA(I),(E(I,J),J=1,N)
100     FORMAT(1X,F10.5,3X,D12.5,' #',8D13.5)
6       CONTINUE
        WRITE(6,125)
125     FORMAT(1X,////)
        DO 7 I=1,N
        WRITE(6,150)(Z(I,J),J=1,4)
150     FORMAT(1X,8D13.5)
7       CONTINUE
        WRITE(6,175)
175     FORMAT(1X,//)
        DO 8 I=1,8
        WRITE(6,150)(Z(I,J),J=5,8)
8       CONTINUE
        WRITE(6,125)
        WRITE(6,200)WK(1),IER
200     FORMAT(1X,/////,D23.16,5X,I5,/,1H1)
13      CONTINUE
        STOP
        END
```

DISTRIBUTION:

DOE/TIC-4500-R67 UC-94b (183)

Texas A&M Research Foundation (2)
FE Box H
College Station, TX   77843

Texas A&M University (5)
Department of Mechanical Engineering
College Station, TX   77843
Attn: J. H. Vance

Lawrence Livermore Laboratory (25)
P. O. Box 808
Livermore, CA   94550
Attn: T. M. Barlow   MS L-388
        D. M. King   MS L-388

U.S. Department of Energy (2)
Division of Energy Storage Systems
600 East St. NW.
Washington, D.C.   20585
Attn: J. H. Swisher
        P. Thompson

U.S. Department of Energy (2)
Division of Distributed Solar Technology
600 East St. NW.
Washington, D.C.   20585
Attn: R. L. San Martin
        P. D. Maycock

Dr. Richard Schneider
Professor, Nuclear Engineering
University of Florida
Gainesville, FL   32611

Mr. B. Dudley Carter
Research Associate
Nuclear Engineering
University of Florida
Gainesville, FL   32611

Mr. Brian Murphy
Research Associate
Mechanical Engineering
Texas A&M University
College Station, TX   77843

Mr. Wallace Ables
Mechanical Facilities Engineer
IBM Corporation
Austin, TX   78712

Mr. J. Wylie Harris, Jr.
2027 Bank of the Southwest Bldg.
Houston, TX 77088

Dr. Paul W. Eschenbach
Director of Engineering Research
Deering Milliken Research Corporation
Spartanburg, SC 29301

University of Minnesota (2)
Department of Mechanical Engineering
111 Church St. SE.
Minneapolis, MN 55455
Attn: A. G. Erdman
       D. L. Hagen
       D. A. Frohrib

2320 K. L. Gillespie
2324 R. S. Pinkham
2324 H. E. Schildknecht (5)
4715 R. H. Braasch
4719 D. G. Schueler
4740 R. K. Traeger
4744 H. M. Dodd
4744 B. C. Caskey
5811 L. A. Harrah
8266 E. A. Aas
3144 T. L. Werner (5)
3151 W. L. Gerner (3)
      For DOE/TIC (Unlimited Release)